Predictive scaling laws for spherical rotating dynamos

Ludivine Oruba, Emmanuel Dormy

Geophysical Journal International

Geophys. J. Int. (2014) **198,** 828–847 doi: 10.1093/gji/ggu159

GJI Geomagnetism, rock magnetism and palaeomagnetism

Predictive scaling laws for spherical rotating dynamos

L. Oruba and E. Dormy

MAG (ENS/IPGP), LRA, Département de Physique, Ecole Normale Supérieure, 24*, rue Lhomond, F-*75231 *Paris Cedex* 05*, France.*
E-mail: dormy@phys.ens.fr

Accepted 2014 April 28. Received 2014 April 25; in original form 2013 November 28

SUMMARY

State of the art numerical models of the Geodynamo are still performed in a parameter regime extremely remote from the values relevant to the physics of the Earth's core. In order to establish a connection between dynamo modelling and the geophysical motivation, it is necessary to use scaling laws. Such scaling laws establish the dependence of essential quantities (such as the magnetic field strength) on measured or controlled quantities. They allow for a direct confrontation of advanced models with geophysical constraints.

We combine a numerical approach, based on a multiple linear regression method in the form of power laws, applied to a database of 102 direct numerical simulations (courtesy of U. Christensen), and a physical approach, based on energetics and forces balances.

We show that previous empirical scaling laws for the magnetic field strength essentially reflect the statistical balance between energy production and dissipation for saturated dynamos. Such power based scaling laws are thus necessarily valid for any dynamo in statistical equilibrium and applicable to any numerical model, irrespectively of the dynamo mechanism.

We show that direct numerical fits can provide contradictory results owing to biases in the parameters space covered in the numerics and to the role of *a priori* hypothesis on the fraction of ohmic dissipation.

We introduce predictive scaling laws, that is relations involving input parameters of the governing equations only. We guide our reasoning on physical considerations. We show that our predictive scaling laws can properly describe the numerical database and reflect the dominant forces balance at work in these numerical simulations. We highlight the dependence of the magnetic field strength on the rotation rate. Finally, our results stress that available numerical models operate in a viscous dynamical regime, which is not relevant to the Earth's core.

Key words: Dynamo: theories and simulations; Geomagnetic induction.

1 INTRODUCTION

Many numerical models have been produced over the last few years to try and reproduce characteristics of planetary and stellar magnetic fields. The parameter regime relevant to these natural objects is however out of reach of present days computational resources. In order to assess the reliability of current numerical models and their relevance to natural applications, it is thus necessary to rely on scaling laws, which can be established on the basis of a set of numerical models with varying control parameters and then extended to the regime of geophysical or astrophysical relevance.

Previous empirical scaling laws for the magnetic field strength (Christensen & Aubert 2006) have proven to be remarkably robust. Indeed they seem to be applicable to numerical models irrespectively of the parameter regime, viscous or inertial (Christensen 2010; Schrinner *et al.* 2012), as well as to natural objects of very different kinds (Christensen *et al.* 2009). Such scaling laws are constructed on the basis of a statistical balance between energy production and dissipation. It is essential to separate the relative importance of this general assumption – which will necessarily be valid for any dynamo in statistical equilibrium – from additional assumptions which could test the nature of a particular dynamo. An additional key issue is that such existing relations only relate measured quantity. They have no predictive power for numerical models in the sense that the knowledge of control parameters (entering the governing equations) is not sufficient to *a priori* estimate the strength of the produced magnetic field. We therefore want to introduce predictive scaling laws, which *a priori* estimate the amplitude of a measured quantity (say the magnetic field strength) as a function of input parameters only.

2 GOVERNING EQUATIONS AND NUMERICAL MODELS

We restrict our study to Boussinesq models of planetary dynamos. The domain consists of a spherical shell, and the aspect ratio between the two bounding spheres is set to $\xi \equiv r_i/r_o = 0.35$. The flow is driven by an imposed difference of temperature between the inner and outer boundaries.

The governing equations in the rotating reference frame can then be written – using $L = r_o - r_i$ as unit of length, Ω^{-1} as unit of time, ΔT as unit of temperature, and $\sqrt{\rho\mu}\,\Omega L$ as unit for the magnetic field – as

$$\partial_t \mathbf{u}^\star + (\mathbf{u}^\star \cdot \boldsymbol{\nabla})\mathbf{u}^\star = -\boldsymbol{\nabla}\pi^\star + \mathrm{E}\,\Delta\mathbf{u}^\star - 2\mathbf{e}_z \times \mathbf{u}^\star + \frac{\mathrm{Ra}\,\mathrm{E}^2}{\mathrm{Pr}}\, T^\star \frac{\mathbf{r}}{r_o} + (\boldsymbol{\nabla} \times \mathbf{B}^\star) \times \mathbf{B}^\star, \tag{1}$$

$$\partial_t \mathbf{B}^\star = \boldsymbol{\nabla} \times (\mathbf{u}^\star \times \mathbf{B}^\star) + \frac{\mathrm{E}}{\mathrm{Pm}}\,\Delta\mathbf{B}^\star,$$

$$\partial_t T^\star + (\mathbf{u}^\star \cdot \boldsymbol{\nabla})T^\star = \frac{\mathrm{E}}{\mathrm{Pr}}\Delta T^\star, \tag{2}$$

$$\boldsymbol{\nabla} \cdot \mathbf{u}^\star = \boldsymbol{\nabla} \cdot \mathbf{B}^\star = 0\,. \tag{3}$$

Because the governing equations involve nine independent physical parameters ($\alpha, g_0, \Delta T, \nu, \kappa, \eta, \Omega, \rho, \mu$) and five units (kg, m, s, K, C), owing to the Buckingham π theorem, only four independent non-dimensional parameters can be introduced. In our system (eqs 1–3), they are the Ekman number $\mathrm{E} = \nu/(\Omega L^2)$, the Prandtl number $\mathrm{Pr} = \nu/\kappa$, the magnetic Prandtl number $\mathrm{Pm} = \nu/\eta$, and the Rayleigh number $\mathrm{Ra} = \alpha g_0 \Delta T L^3/(\nu\kappa)$, in which ν is the kinematic viscosity of the fluid, α the coefficient of thermal expansion, g_0 the gravity at the outer bounding sphere, $\kappa = k/(\rho c)$ its thermal diffusivity, and η its magnetic diffusivity. Throughout this article, non-dimensional quantities are denoted with a *.

All the simulations used in this work rely on no-slip mechanical boundary conditions and an insulating outer domain. The inner core is insulating in most simulations, and a few simulations involve a conducting inner core with the same conductivity as the fluid.

Our analysis will be tested against a wide database of 185 direct numerical simulations kindly provided by U. Christensen. The data sample is reduced to 102 to only take into account dynamo simulations corresponding to fully developed convection ($\mathrm{Nu} > 2$) and producing a dipolar magnetic field (relative dipole field strength f_{dip} larger than 0.5). Moreover, we limit our study to $\mathrm{Pr} \leq 10$, that is to say to values not too far from the value estimated for the Earth's core. We will also highlight the subset of this database which was used in Christensen & Aubert (2006). It is composed of 65 runs available at the time. Finally we will use a few additional numerical data published in Morin & Dormy (2009).

These numerical data can be used to test scaling laws guided by physical reasoning. It can also be used to establish direct numerical fits. To this end, we introduce a multiple linear regression approach (Montgomery *et al.* 2001; Cornillon & Matzner-Lober 2010), detailed in Appendix A.

3 POWER BASED SCALINGS, KEY PARAMETERS AND THEIR RELATIONS

3.1 Energy balance between production and dissipation

In order to derive a scaling law for the magnetic field strength, a possible approach introduced by Christensen & Aubert (2006) is to consider the statistical balance between energy production by buoyancy forces and dissipation. Time averaged quantities of a statistically steady dynamo state should obviously satisfy

$$\mathrm{P} = D_\eta + D_\nu, \tag{4}$$

where P is the power generated by buoyancy forces, D_η is the rate of ohmic dissipation

$$D_\eta = \int_V \frac{\eta}{\mu}\,(\boldsymbol{\nabla}\times\mathbf{B})^2\,\mathrm{d}V, \qquad \text{that is} \quad D_\eta^\star = \mathrm{E}_\eta \int_V (\boldsymbol{\nabla}\times\mathbf{B}^\star)^2\,\mathrm{d}V^\star,$$

in which $\mathrm{E}_\eta = \mathrm{E}/\mathrm{Pm}$ is the magnetic Ekman number and D_ν is the rate of viscous dissipation

$$D_\nu = \int_V \rho\nu\,(\boldsymbol{\nabla}\times\mathbf{u})^2\,\mathrm{d}V, \qquad \text{that is} \quad D_\nu^\star = \mathrm{E} \int_V (\boldsymbol{\nabla}\times\mathbf{u}^\star)^2\,\mathrm{d}V^\star\,.$$

The above quantities are all defined as time averaged over a sufficient amount of time, so that they are steady for a given parameter set.

Following Christensen & Aubert (2006) and introducing the f_{ohm} coefficient, defined as

$$f_{\mathrm{ohm}} \equiv \frac{D_\eta}{D_\eta + D_\nu}, \tag{5}$$

we get

$$\mathrm{P} = \frac{D_\eta}{f_{\mathrm{ohm}}} = \frac{1}{f_{\mathrm{ohm}}} \int_V \frac{\eta}{\mu}\,(\boldsymbol{\nabla}\times\mathbf{B})^2\,\mathrm{d}V \sim \frac{1}{f_{\mathrm{ohm}}}\,\frac{\eta}{\mu}\,\frac{\mathrm{B}^2}{\ell_B^2}\,V, \tag{6}$$

where we introduced a typical magnetic field strength B and a magnetic dissipation length scale ℓ_B, defined again using time averaged quantities as

$$\ell_B^2 \equiv \frac{\int_V \mathbf{B}^2\,\mathrm{d}V}{\int_V (\boldsymbol{\nabla}\times\mathbf{B})^2\,\mathrm{d}V} = 2\,\eta\,\frac{\mathrm{E}_{\mathrm{mag}}}{D_\eta} \qquad \text{that is} \qquad \ell_B^{\star\,2} \equiv 2\,\mathrm{E}_\eta\,\frac{\mathrm{E}_{\mathrm{mag}}^\star}{D_\eta^\star}, \tag{7}$$

$$\text{with} \qquad \mathrm{E}_{\mathrm{mag}} = \int_V \frac{\mathbf{B}^2}{2\mu}\,\mathrm{d}V, \qquad \text{that is} \qquad \mathrm{E}_{\mathrm{mag}}^\star = \int_V \frac{\mathbf{B}^{\star 2}}{2}\,\mathrm{d}V^\star. \tag{8}$$

This simple reasoning provides the following expression for the magnetic field strength

$$\frac{\mathrm{B}^2}{\mu} \sim f_{\mathrm{ohm}}\,\ell_B^2\,\frac{\mathrm{P}}{\eta\,V} = f_{\mathrm{ohm}}\,\ell_B^2\,\frac{\rho\,\mathrm{P}_M}{\eta}, \tag{9}$$

where P_M is the mass power generated by buoyancy forces $\mathrm{P}_M \equiv \mathrm{P}/(\rho V)$.

The non-dimensional form of eq. (9) is

$$\mathrm{Lo} \sim {f_{\mathrm{ohm}}}^{1/2}\,\mathrm{P}^{\star 1/2}\,\mathrm{E}_\eta^{-1/2}\,\ell_B^\star, \tag{10}$$

where $\mathrm{Lo} \equiv \left(2\,{\mathrm{E}_{\mathrm{mag}}}^\star/V^\star\right)^{\frac{1}{2}} \equiv \mathrm{B}^\star$. Expressing a scaling law for B (or its non-dimensional form Lo) therefore reduces to relating P and ℓ_B to the relevant parameters.

In previous studies ℓ_B has often not been introduced as such (but see the review by Roberts & King 2013). Instead it is usually indirectly evaluated by introducing the magnetic dissipation time $\tau_{\mathrm{diss}} \equiv \mathrm{E}_{\mathrm{mag}}/D_\eta = \ell_B^2/(2\eta)$ (see Christensen & Tilgner 2004), or in non-dimensional form $\tau_\eta^\star \equiv \tau_{\mathrm{diss}}/\tau_{\mathrm{dip}}$, where $\tau_{\mathrm{dip}} \equiv L^2/(\pi^2\,\eta)$. This definition leads to $\tau_\eta^\star = \pi^2/2\;{\ell_B^\star}^2$. Besides, the parameter f_{ohm} is a rather complex number, which involves both *a priori* input and *a posteriori* output model properties. It is usually assumed to be order one in natural dynamos (but see Schrinner 2013), its importance in scaling laws is discussed in Appendix B.

3.2 Power generated by buoyancy forces

Christensen & Aubert (2006) established a relation between $\mathrm{P}^\star$ and a flux-based Rayleigh number $\mathrm{Ra}_Q^\star$

$$\mathrm{Ra}_Q^\star \equiv \frac{1}{4\pi\, r_o\, r_i}\, \frac{\alpha\, g\, r_o\, \Delta Q}{\rho\, c\, \Omega^3\, (r_o - r_i)^2}, \tag{11}$$

where ΔQ is the difference between the time-average total heat flow Q and $Q_d^{T_s} = 4\pi k T_a$ $(J \cdot s^{-1})$, which corresponds to the diffusive heat flow associated to $T_S(r) = T_a/r + T_b$.

They show that

$$\mathrm{P}^\star \approx 2\pi\, \xi\, \frac{1+\xi}{(1-\xi)^2}\, \mathrm{Ra}_Q^\star, \tag{12}$$

under the assumptions that the volume integral of the realized temperature gradient can be approximated by its conductive counterpart. The demonstration requires in particular fixed temperature boundary conditions. Relation (12) is well verified for the numerical database used in this study. That is why in the following numerical analysis of scaling laws, the parameter $\mathrm{P}^\star$ will be replaced by $\mathrm{Ra}_Q^\star$ with a pre-factor of 7.03 determined by the geometry via the aspect ratio ξ.

It is important to stress that $\mathrm{Ra}_Q^\star$ is an output parameter, and cannot be controlled *a priori* when using fixed temperature boundary conditions. It can however be related to the classical Rayleigh number, which is a control parameter of the problem. Indeed, introducing the Nusselt number $\mathrm{Nu} \equiv Q/Q_d^{T_s}$, which can be rewritten as $\mathrm{Nu} = Q_d(r_o)/(4\pi k T_a)$ under the statistically steady assumption, relation (11) becomes

$$\mathrm{Ra}_Q^\star = \mathrm{E}^3\, \mathrm{Pr}^{-2}\, \mathrm{Ra}\, (\mathrm{Nu} - 1)\,. \tag{13}$$

The $\mathrm{Ra}_Q^\star$ parameter can not be controlled in the problem because it is related to the output parameter Nu. Its value is zero at the onset of convection ($\mathrm{Nu} = 1$).

Note that $\mathrm{Ra}_Q^\star\, \mathrm{Nu}/(\mathrm{Nu} - 1)$ would be an input control parameter in the case of imposed heat flux boundary conditions. The construction of $\mathrm{Ra}_Q^\star$ would however still involve, even with such boundary conditions, measurements of the Nusselt number, because the temperature difference across the shell becomes a measured quantity.

3.3 Role of the magnetic dissipation length scale ℓ_B

In the numerical database used in this paper, the dissipation length scale $\ell_B^\star$, calculated using eq. (7), varies between 0.02 and 0.10. These values are obviously smaller than those corresponding to the pure dipole decay in the absence of motions $\tau_\eta^\star = 1/2$, that is $\ell_B^\star = 1/\pi \simeq 0.30$. Besides, the range of variation of $\ell_B^\star$ is less than one order of magnitude. Thus, as a first approximation, the variations of $\ell_B^\star$ can be neglected, namely it can be set to a constant in eq. (10). Using the relation (12), eq. (10) becomes under this assumption

$$\mathrm{Lo} \sim {f_{\mathrm{ohm}}}^{1/2} \mathrm{Ra}_Q^{\star\, 1/2}\, \mathrm{E}_\eta^{-1/2}\,. \tag{14}$$

Its application to the 102 dynamos database is represented in Fig. 1, and yields the relative misfit $\chi_{\mathrm{rel}} = 0.433$. Relation (14), which simply corresponds to the energy balance between production and dissipation with ℓ_B approximated as a constant, already provides a good fit to the numerical data. This implies that empirical fits of the magnetic field strength previously obtained in the literature mainly reflect this simple balance between energy production and dissipation, combined with an improved description of the magnetic dissipation ℓ_B than a simple constant, which is however not essential.

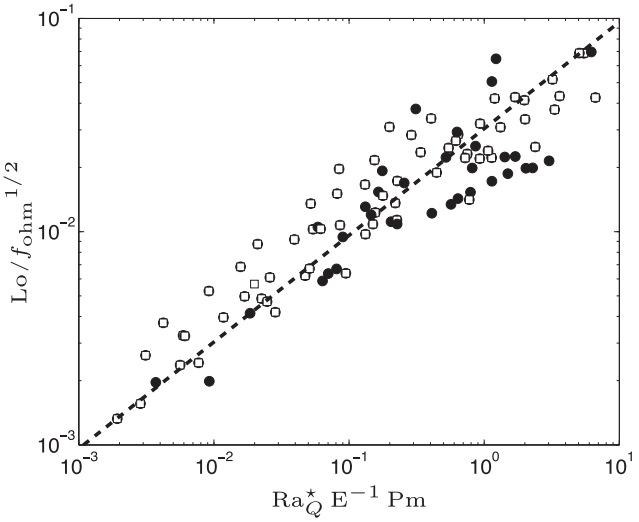

Figure 1. The Lorentz number corrected for the relative fraction of Ohmic dissipation versus a combination of the flux-based Rayleigh number, the Ekman number and the magnetic Prandtl number: eq. (14). This simple scaling law only reflects the statistical balance between energy production and dissipation, combined with a constant ℓ_B. Points correspond to the full 102 dynamos database, open squares indicate the subset used in Christensen & Aubert (2006).

The statistical balance between both terms of the right-hand side of the dimensional form of the induction eq. (2) yields to $\mathrm{uB}/\ell \sim \eta \mathrm{B}/\ell_B^2$, where we introduced a typical velocity field strength u, and ℓ has the dimension of a length scale which depends on correlations between the norm and direction of $\mathbf{u}$ and $\mathbf{B}$. The length scales ℓ_B and ℓ are thus related by

$$\ell_B \sim \eta^{1/2}\, \mathrm{u}^{-1/2}\, \ell^{1/2}, \tag{15}$$

which can be normalized as

$$\ell_B^\star \sim \mathrm{Rm}^{-1/2}\, \ell^{\star 1/2}, \qquad \text{or} \qquad \ell_B^\star \sim \mathrm{E}_\eta^{1/2}\, \mathrm{Ro}^{-1/2}\, \ell^{\star 1/2}, \tag{16}$$

where Rm is the magnetic Reynolds number, and Ro is the Rossby number, defined as $\mathrm{Ro} \equiv (2\, \mathrm{E_{kin}}^\star / V^\star)^{\frac{1}{2}} \equiv u^\star$,

$$\text{with} \qquad \mathrm{E_{kin}} \equiv \int_V \frac{\rho\, \mathbf{u}^2}{2}\, \mathrm{d}V, \qquad \text{that is} \qquad \mathrm{E_{kin}^\star} \equiv \int_V \frac{\mathbf{u}^{\star 2}}{2}\, \mathrm{d}V^\star. \tag{17}$$

The magnetic dissipation length scale ℓ_B is thus an output parameter, in so far as it is related to both the characteristic velocity u of the flow (measured by Ro or Rm) and the length scale ℓ (see Appendix C1).

3.4 Existing scaling laws for the magnetic field strength and their physical interpretation

Christensen & Aubert (2006) introduced two seminal scaling laws

$$\mathrm{Lo} \sim {f_{\mathrm{ohm}}}^{1/2}\, \mathrm{Ra}_Q^{\star\, 0.34}\,, \tag{18}$$

and its optimised form

$$\mathrm{Lo} \sim {f_{\mathrm{ohm}}}^{1/2}\, \mathrm{Ra}_Q^{\star\, 0.32}\, \mathrm{Pm}^{0.11}\,. \tag{19}$$

Their application to the 102 dynamos database is represented in Fig. 2, and yields the relative misfits $\chi_{\mathrm{rel}} = 0.256$ and $\chi_{\mathrm{rel}} = 0.152$, respectively. The corresponding assumption on the magnetic dissipation length scale $\ell_B^\star$ is detailed in Appendix C2. It respectively

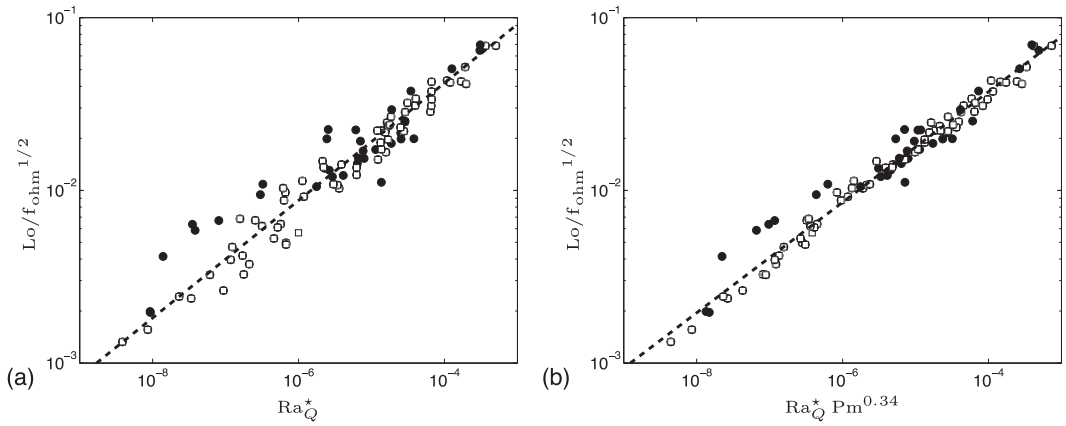

Figure 2. The Lorentz number corrected for the relative fraction of Ohmic dissipation versus a combination of the flux-based Rayleigh number and the magnetic Prandtl number, as proposed by Christensen & Aubert (2006): (a) relation (18), (b) relation (19). Blacks points correspond to the 102 dynamos database, open squares indicate the subset of data used in Christensen & Aubert (2006).

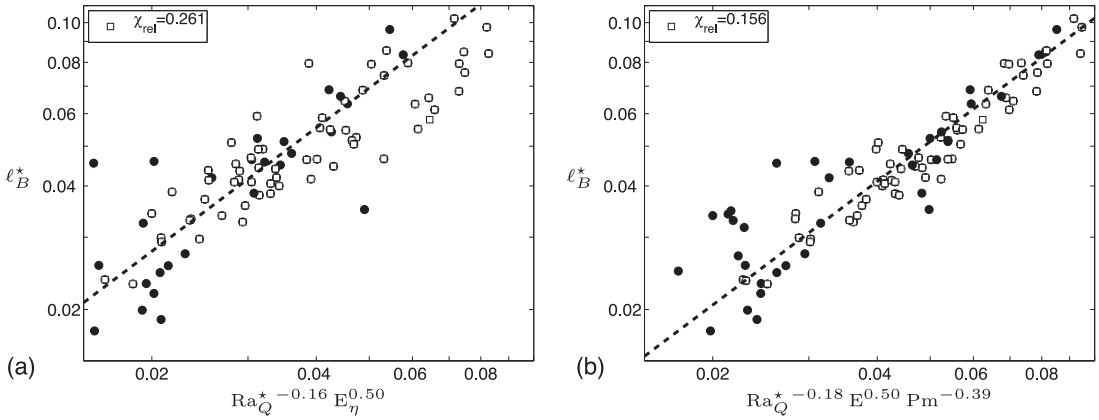

Figure 3. The magnetic dissipation length scale versus a combination of the flux-based Rayleigh number, the Ekman number and the magnetic Prandtl number, as implied by Christensen & Aubert (2006) results (relations 20). Black points correspond to the full 102 dynamos database, open squares indicate the subset used in Christensen & Aubert (2006).

yields

$$\ell_B^\star \sim \mathrm{Ra}_Q^{\star\,-0.16}\,\mathrm{E}_\eta^{1/2}, \qquad \text{and} \qquad \ell_B^\star \sim \mathrm{Ra}_Q^{\star\,-0.18}\,\mathrm{E}^{1/2}\,\mathrm{Pm}^{-0.39}, \tag{20}$$

which are represented in Fig. 3 (see Appendix C2 for discussion).

Relation (18) and its optimized form (19) are empirical laws obtained using numerical experiments. The physical interpretation of relation (18), as provided by Christensen & Aubert (2006), is based on two assumptions: the empirical scaling law for the magnetic dissipation time $\tau_\eta^\star \sim \mathrm{Rm}^{-1}$ (Christensen & Tilgner 2004), which is equivalent to assuming $\ell^\star \sim 1$ (see Appendix C1), and their empirical fit $\mathrm{Ro} \sim \mathrm{Ra}_Q^{\star\,0.41}$ (eq. 30 in Christensen & Aubert 2006). Using eq. (16), these two assumptions provide $\ell_B^\star \sim \mathrm{Ra}_Q^{\star\,-0.21}\,\mathrm{E}_\eta^{1/2}$. This last expression can then be injected in eq. (10), to yield $\mathrm{Lo} \sim {f_\mathrm{ohm}}^{1/2}\,\mathrm{Ra}_Q^{\star\,0.29}$. Thus, their demonstration leads to an exponent of $\mathrm{Ra}_Q^\star$ equal to 0.29, which is only slightly lower than their optimal exponent 0.34 in (18).

Christensen (2010) proposed a modified interpretation: while retaining the assumption $\ell^\star \sim 1$, he replaced the scaling law for Ro by the one resulting from mixing length theory (balance between inertia and buoyancy). This theory, usually applied for turbulent convection in stars (Stevenson 1979; Kippenham & Weigert 1990), provides $\mathrm{Ro} \sim \mathrm{Ra}_Q^{\star\,1/3}$. It leads to $\mathrm{Lo} \sim {f_\mathrm{ohm}}^{1/2}\,\mathrm{Ra}_Q^{\star\,1/3}$, which is closer to the original fit (18) obtained by Christensen & Aubert (2006). Instead, Jones (2011) based his physical reasoning on the inertial scaling law $\mathrm{Ro} \sim \mathrm{Ra}_Q^{\star\,2/5}$ (derived from the so-called IAC balance, see Aubert *et al.* 2001), and obtained $\mathrm{Lo} \sim {f_\mathrm{ohm}}^{1/2}\,\mathrm{Ra}_Q^{\star\,0.30}$. The assumptions of inertial scaling laws for Ro made by both Christensen (2010) and Jones (2011) however do not seem relevant to dipolar numerical dynamos (see Section 4.5 of this paper; and Christensen & Aubert 2006; Soderlund *et al.* 2012).

More recently, Davidson (2013) studied analytically the asymptotic limit expected to be relevant to planetary dynamos. In this limit, viscosity is negligible, which implies a vanishing viscous dissipation ($f_\mathrm{ohm} \sim 1$), and inertial forces do not enter the dominant forces balance (small Rossby number limit). Davidson's argument relies on a dimensional analysis. On the right-hand side of eq. (9), with $f_\mathrm{ohm} = 1$, both P_M and ℓ_B^2/η are assumed to be independent on Ω. This implies that $B^2/(\rho\mu)$ only depends on L and P_M, and thus

$$\frac{\mathrm{B}^2}{\rho\,\mu} \sim L^{2/3}\,{\mathrm{P}_M}^{2/3}, \tag{21}$$

(see eq. 6 in Davidson 2013). In order to account for viscous effects in numerical simulations, Davidson (2013) then replaces P_M with $f_\mathrm{ohm}\mathrm{P}_M$ in (21), which leads to

$$\frac{\mathrm{B}^2}{\rho\,\mu} \sim L^{2/3}\,(f_\mathrm{ohm}\,\mathrm{P}_M)^{2/3}, \tag{22}$$

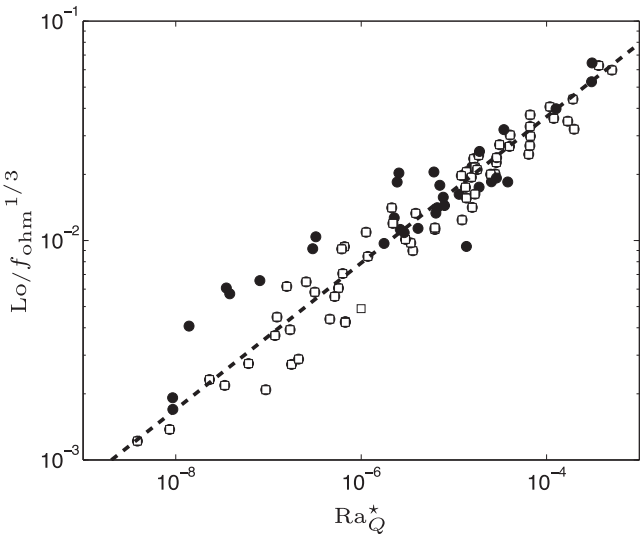

Figure 4. The Lorentz number corrected for the relative fraction of Ohmic dissipation versus a combination of the flux-based Rayleigh number and the magnetic Prandtl number, as proposed by Davidson (2013), relation (23). Blacks points correspond to the 102 dynamos database, open squares indicate the subset of data used in Christensen & Aubert (2006).

(eq. 9 in Davidson 2013). It can be rewritten in its non-dimensional form as

$$\mathrm{Lo} \sim {f_{\mathrm{ohm}}}^{1/3}\, {\mathrm{Ra}^{\star}_{Q}}^{1/3}. \tag{23}$$

Note that relation (23) is based on physical considerations valid for the Earth's core but not necessarily realized in direct numerical simulations (see Appendix D). It is similar to (18) except for the exponent of f_{ohm}. The importance of this measured quantity in the efficiency of the power based scaling laws is investigated in Appendix B. Its application to the 102 dynamos database is represented in Fig. 4, and yields a relative misfit $\chi_{\mathrm{rel}} = 0.286$.

We discussed above three scaling laws proposed for the magnetic field strength primarily as a function of the available power generated by buoyancy forces and corresponding to eqs (18), (19) and (23). Their application to our dynamos database is represented in Figs 2 and 4. Note that extending the 65 dynamos database of Christensen & Aubert (2006) to the 102 dynamos database provided by U. Christensen and used in the present paper, leads to a lower quality fit for the magnetic field amplitude (compare figs 8–9 in Christensen & Aubert 2006, with Figs 2a and b in this paper). The three relations offer a good description of the available numerical data, with relative misfits between 0.15 and 0.30. The best one is naturally relation (19), since it involves a supplementary parameter Pm compared to scaling laws (18) and (23).

It is interesting to compare these three relations with the most simple form which stems from the energy balance between production and dissipation and the assumption that ℓ_B is constant (dominant dipole field). This expression is represented in Fig. 1 (see also eq. 14). The relative misfit is only improved by some 50 per cent from this last relation to relations (18), (19) and (23) which all attempt to a finer description of the magnetic dissipation length scale. The range of variation of ℓ_B in numerical models is necessarily restricted between the discretisation size and the size L of the model. The key assumption is thus the statistical balance between energy production and dissipation, which is bound to work for any statistically steady dynamo (as illustrated in Fig. 1). This explains why the power based scaling law (18) was found to work with different prefactors for dipolar and multipolar dynamos, despite of their different induction mechanisms (Christensen 2010; Schrinner *et al.* 2012).

4 PREDICTIVE SCALING LAWS FOR THE MAGNETIC FIELD STRENGTH

Power based scaling laws, discussed in the previous section, properly describe the numerical database. However they only relate together measured quantities. We now want to express scaling laws which only involve input parameters on the right-hand side. Such scaling laws will be referred to as 'predictive' in the sense that they estimate the strength of a measured quantity, say the magnetic field strength, as a function of input parameters only (i.e. parameters that explicitely enter the governing equations), and can therefore be used before any simulation is performed (as opposed to scaling laws involving measured quantities such as $\mathrm{Ra}^{\star}_{Q}$ and f_{ohm}).

4.1 Control parameters

Only four non-dimensional parameters can be introduced in the governing equations (1–3). In our formulation, these are the Ekman number E, the Prandtl number Pr, the magnetic Prandtl number Pm and the Rayleigh number Ra (see Section 2). According to the Buckingham π theorem, any additional non-dimensional quantity, for example the Elsasser number $\Lambda \equiv \mathrm{Lo}^2\mathrm{Pm}/\mathrm{E}$, can therefore be expressed as a function of the above four non-dimensional control parameters. The choice of non-dimensional parameters is however non-unique (for example, the Roberts number $\mathrm{q} = \kappa/\eta$ could be used instead of the magnetic Prandtl number $\mathrm{Pm} = \nu/\eta$).

Stelzer & Jackson (2013) opened the way to a predictive scaling by expressing $\mathrm{Nu} - 1$, Ro and $\mathrm{Lo}/{f_{\mathrm{ohm}}}^{1/2}$ as a function of Ra instead of $\mathrm{Ra}^{\star}_{Q}$ (see their section 5). Their approach however is bound to fail for small values of Ra as all these measured quantities obviously vanish below the onset of convection or dynamo action.

Instead of using the Rayleigh number as control parameter, it is thus natural to introduce the distance to an instability threshold. We thus introduce Ra_c and Ra_d, which respectively correspond to the onset of convection and dynamo action (see Appendix E for Ra_d). The measured quantities $\mathrm{Nu} - 1$ and Ro are expected to vanish at the onset of convection $\mathrm{Ra} = \mathrm{Ra}_c$ and Lo at the onset of dynamo action $\mathrm{Ra} = \mathrm{Ra}_d$.

The quantity $\mathrm{Ra} - \mathrm{Ra}_c$ therefore provides a natural control parameter for hydrodynamic quantities such as $\mathrm{Nu} - 1$ and Ro. This control parameter, even though natural, is however biased because of the strong dependence of the critical Rayleigh number Ra_c on E and Pr. This dependence, first formulated and investigated by Chandrasekhar (1961) in the cartesian geometry, has been extensively studied. Especially, Roberts (1968) then Busse (1970) studied the limit $\mathrm{E} \ll 1$ in a spherical geometry. In a perturbative cylindric model for a uniformly heated fluid, Busse (1970) proposed

$$\mathrm{Ra}_c \sim \mathrm{E}^{-4/3} \left(\frac{\mathrm{Pr}}{1+\mathrm{Pr}}\right)^{4/3}. \tag{24}$$

This solution, valid in the limit of asymptotic Ekman numbers, is consistent with several other studies: for example, Carrigan & Busse (1983) (experimental convection study in a differentially heated spherical shell), Jones *et al.* (2000) (uniformly heated fluid in a sphere), Takehiro *et al.* (2002) (fixed heat flux boundary conditions), Dormy *et al.* (2004) and Zhang & Liao (2004). It is validated to a certain extent against the finite Ekman number numerical database

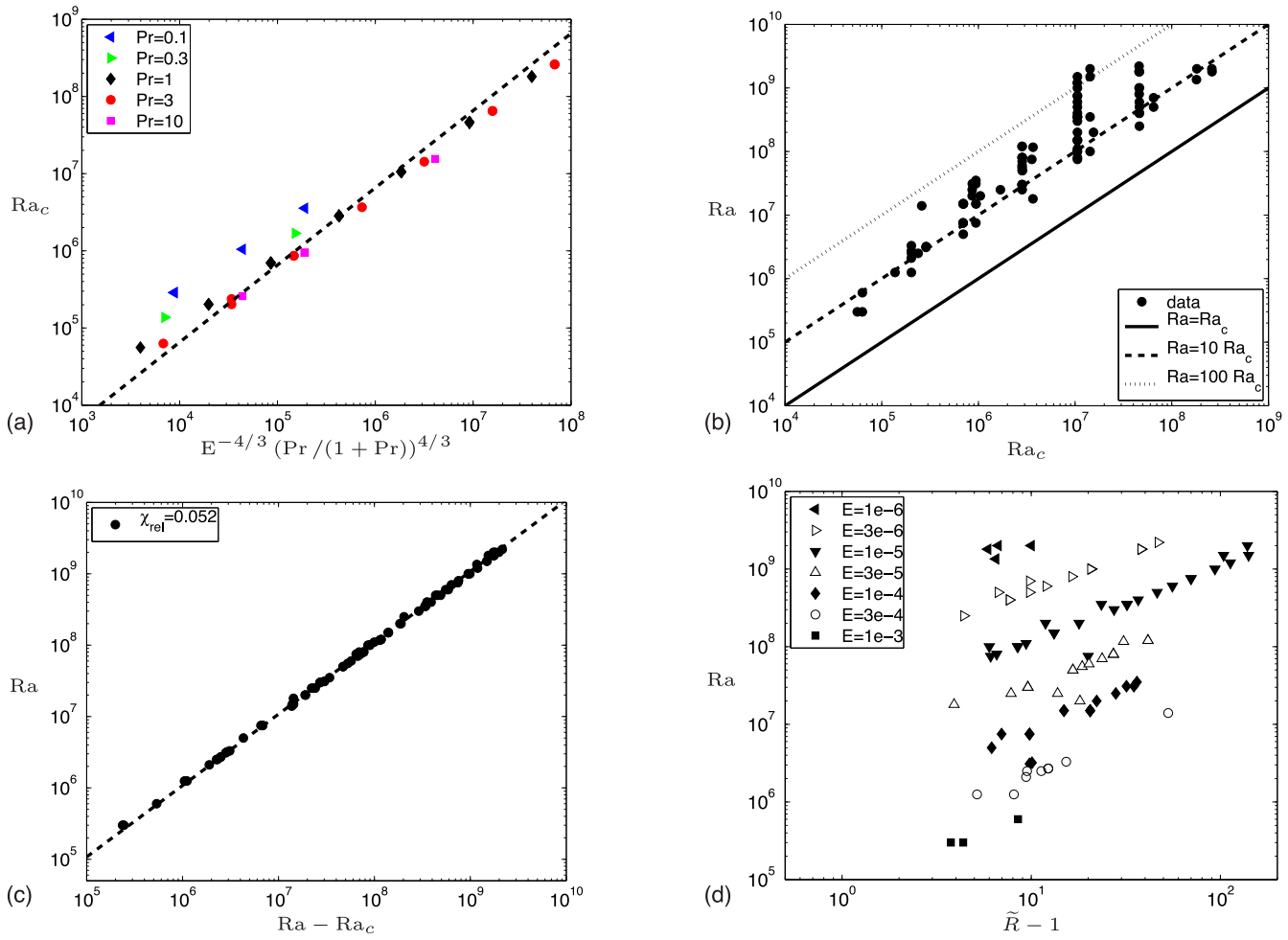

Figure 5. (a) The critical Rayleigh number for the onset of convection versus the predicted combination of the Ekman number and the Prandtl number (Busse 1970). (b) Parameter range: Rayleigh number in ordinate, critical Rayleigh number for convection in abscissa. (c) The strong correlation in the database between the Rayleigh number and its distance to the onset of convection. (d) The Rayleigh number versus its normalized distance to the onset of convection. The four graphs rely on the 102 dynamos database.

used in this paper. The corresponding misfit is $\chi_{\rm rel} = 0.319$ and it is represented in Fig. 5(a). Note that a dependence on $\mathrm{Pr}/(1+\mathrm{Pr})$ remains. The optimised scaling law obtained with our database is $\mathrm{Ra}_c \simeq 17.78\,\mathrm{E}^{-1.19}\,[\mathrm{Pr}/(1+\mathrm{Pr})]^{0.58}$, with $\chi_{\rm rel} = 0.061$ (95 per cent confidence intervals in Table 2): optimized exponents are slightly weaker (in absolute value) than those predicted by the asymptotic calculus of Busse (1970), which indicates that these models are still not in an asymptotic limit.

In practice, the numerical experiments used in this study are performed for values of Ra of the order of 10 times the critical value (see Fig. 5b). Indeed, only dynamos with $\mathrm{Nu} > 2$ are considered in the database (see Christensen & Aubert 2006), on the other hand, for obvious computational reasons associated with small scale motions, Ra is never very far from the onset in numerical models. As a result, the values of Ra are strongly correlated with the values of Ra_c. It follows that Ra is in fact close to $\mathrm{Ra} - \mathrm{Ra}_c$: in the numerical database, $\mathrm{Ra} \approx 1.11(\mathrm{Ra} - \mathrm{Ra}_c)$ with a relative misfit $\chi_{\rm rel} = 0.052$ (see Fig. 5c). This last relation, which traduces a bias in the database, explains why Stelzer & Jackson (2013) obtained satisfying fits of Ro and $\mathrm{Nu} - 1$ as a function of Ra (without introducing the distance to the onset of convection).

The strong dependence of Ra_c on the Ekman number introduces a very large variation of the control parameter $\mathrm{Ra} - \mathrm{Ra}_c$, spanning over five orders of magnitude in the numerical database. This is somewhat fictitious as the parameter $\mathrm{Ra}/\mathrm{Ra}_c$ would only vary over one order of magnitude. We thus introduce $\widetilde{R} \equiv \mathrm{Ra}/\mathrm{Ra}_c$ and our new control parameter will thus be $\widetilde{R} - 1$ (as $\widetilde{R}_c = 1$). This new control parameter filters out the Ekman and Prandtl number dependences (the Ekman dependence is highlighted in Fig. 5d).

To measure the distance to the onset of dynamo action, we also introduce the control parameter $\widetilde{R} - \widetilde{R}_d$, where $\widetilde{R}_d \equiv \mathrm{Ra}_d/\mathrm{Ra}_c$ is a function of E, Pr and Pm only. Nevertheless, whereas Ra_c is known for all numerical experiments in the database provided by U. Christensen, this is not the case for the critical value at the onset of dynamo action Ra_d. It can be estimated through a linear interpolation of Lo^2 as a function of Ra near the onset of dynamo action (see Appendix E). Such an estimate could only be performed for seven sets of E, Pr and Pm in the database (see Table 1), which corresponds to 33 numerical simulations. It is extended to 42 simulations thanks to nine additional direct numerical simulations extracted from Morin & Dormy (2009) and corresponding to the set $\mathrm{E} = 3 \times 10^{-4}$, $\mathrm{Pr} = 1$ and $\mathrm{Pm} = 3$.

Our four control parameters therefore are: the Ekman number E, the Prandtl number Pr, the magnetic Prandtl number Pm and the relative distance to either the onset of convection or of dynamo action, $\widetilde{R} - 1$ and $\widetilde{R} - \widetilde{R}_d$, respectively.

Table 1. Estimated values of the Rayleigh number and of the magnetic Reynolds number, corresponding to the onset of dynamo action (see Appendix E).

E	Pr	Pm	Ra_d	Rm_d
3×10^{-4}	1	3	6.125×10^5	62.5
1×10^{-4}	1	0.5	3.6×10^6	26
1×10^{-4}	1	1	2.4×10^6	34
1×10^{-4}	10	10	5×10^5	25
3×10^{-5}	1	0.25	2.6×10^7	29
3×10^{-5}	1	1	1.5×10^7	70
3×10^{-5}	1	2.5	1.04×10^7	103
1×10^{-5}	1	0.5	8.0×10^7	70
1×10^{-5}	1	1	4.7×10^7	68
1×10^{-5}	1	2	4.9×10^7	150
3×10^{-6}	1	0.1	6.4×10^8	40
3×10^{-6}	1	0.5	2.4×10^8	60

4.2 Direct numerical fit versus forces balances

Empirical scaling laws deduced from the multiple linear regression method applied to numerical data have to be considered carefully for two main reasons. First, the ranges of some input parameters are highly correlated, which introduces bias in scaling laws. It is the case for the Ekman number and the magnetic Prandtl number. The minimal value of Pm required for dynamo is indeed dependent on E (see Christensen & Aubert 2006). Fig. 6 represents the range of Pm as a function of the range of E in the 102 dymanos database used in this study: the minimal value of Pm varies roughly as $E^{3/4}$ (Christensen *et al.* 1999; Christensen & Aubert 2006), although this cannot be distinguished from $E^{2/3}$ (as proposed by Dormy & Le Mouël 2008). As a consequence, the scaling laws obtained via a direct numerical fit have to be considered carefully. In particular, biases can occur relating dependences on E and Pm.

The second important limit of the approach based on empirical scaling laws deals with the restriction of our scaling analysis to power laws. In particular, the dependence on the Prandtl coefficient seems more complex than a simple power law. For instance, the dependence of the critical Rayleigh number Ra_c on Pr takes the form $Pr/(1 + Pr)$ [see (24) above]. Indeed, a power law expression would diverge in the limit Pr tends to infinity.

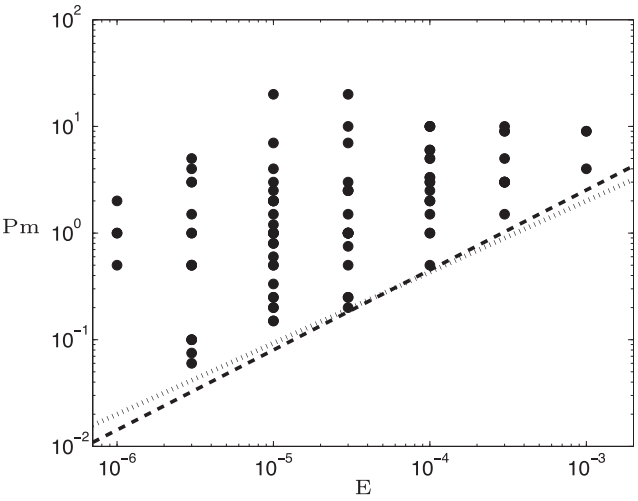

Figure 6. Correlation in control parameters used in numerical models; the magnetic Prandtl number is represented as a function of the Ekman number. The dashed line corresponds to $Pm_{min} = 450\,E^{0.75}$ (Christensen & Aubert 2006) and the dotted line to $Pm_{min} \sim E^{2/3}$ (Dormy & Le Mouël 2008). This figure relies on the full 102 dynamos database.

Because of the above limitations, we prefer to guide our derivation of scaling laws with physical arguments such as forces balances. Our motivation is to take some distance with empirical fits, and to rely on the numerical database to validate the proposed scaling laws, guided by physical arguments.

4.3 Magnetic field strength as a function of the flow amplitude

A first step in our reasoning consists in expressing the magnetic field strength as a function of the flow amplitude. In experimental physics, one usually controls the peak velocity of a flow driven say by propellers. For this reason, earlier theoretical work often focused on the relation between the produced magnetic field and the velocity field. A first approach is to consider dynamos which bifurcate from a laminar flow. One assumes that in such cases, a dominant balance exists between the Lorentz force and the viscous force associated to the flow modification (Petrelis & Fauve 2001).

It yields the equilibrium

$$\mathrm{Lo}^2 \sim \mathrm{E}\,\frac{\mathrm{Ro} - \mathrm{Ro}_d}{\tilde{\ell}_u^{\star 2}}, \tag{25}$$

where Ro_d corresponds to the Rossby number at the onset of dynamo action, and the length scale $\tilde{\ell}_u$ corresponds to the characteristic length scale of the flow calculated as the mean scale of the kinetic energy spectrum (see Christensen & Aubert 2006). This length scale is very similar to our ℓ_u introduced in Appendix B1.

Supposing, as do Petrelis & Fauve (2001), that $\tilde{\ell}_u^{\star} \sim 1$, this leads in non-dimensional form to

$$\Lambda \sim (\mathrm{Rm} - \mathrm{Rm}_d)\,\mathrm{E}, \tag{26}$$

where Rm_d corresponds to the critical value of Rm at the onset of dynamo action.

While the length scale $\tilde{\ell}_u^{\star}$ necessarily varies over a limited range in the numerical database (see Fig. 7a and the discussion at the end of Section 3.4), a finer description can be achieved by retaining viscous effects and neglecting inertial forces. The equilibrium between the curl of the Coriolis force and the viscous force indeed yields

$$\tilde{\ell}_u^{\star} \sim \mathrm{E}^{1/3}. \tag{27}$$

This last relation properly describes the database used in the present paper, as shown in Fig. 7(a) and in King & Buffett (2013) (see also Roberts & King 2013). The lengthscale $\tilde{\ell}_u^{\star}$ clearly depends on $E^{1/3}$ and not on $E^{1/2}$, the latter being the typical scale of boundary layers. Thus, viscous effects play a non-negligible role in the bulk of the flow. This indicates that present numerical simulations are not in a dynamical regime relevant to the Earth's core (see also Soderlund *et al.* 2012). The $E^{1/3}$ scale would represent less than 100 m for geophysical values. Besides, the mild dependence of $\tilde{\ell}_u^{\star}\,\mathrm{E}^{-1/3}$ on the Rossby number (see Fig. 7b) shows that the assumption that inertia is small compared to viscous effects is verified by numerical models.

If one uses (27) for the length scale $\tilde{\ell}_u^{\star}$ in relation (25) (see Fauve & Petrelis 2007), this yields

$$\Lambda \sim (\mathrm{Rm} - \mathrm{Rm}_d)\,\mathrm{E}^{1/3}. \tag{28}$$

An alternative forces balance, known as the strong field balance, and assumed to be valid for the Earth's core, consists in assuming a balance between the Lorentz force and the modification of the

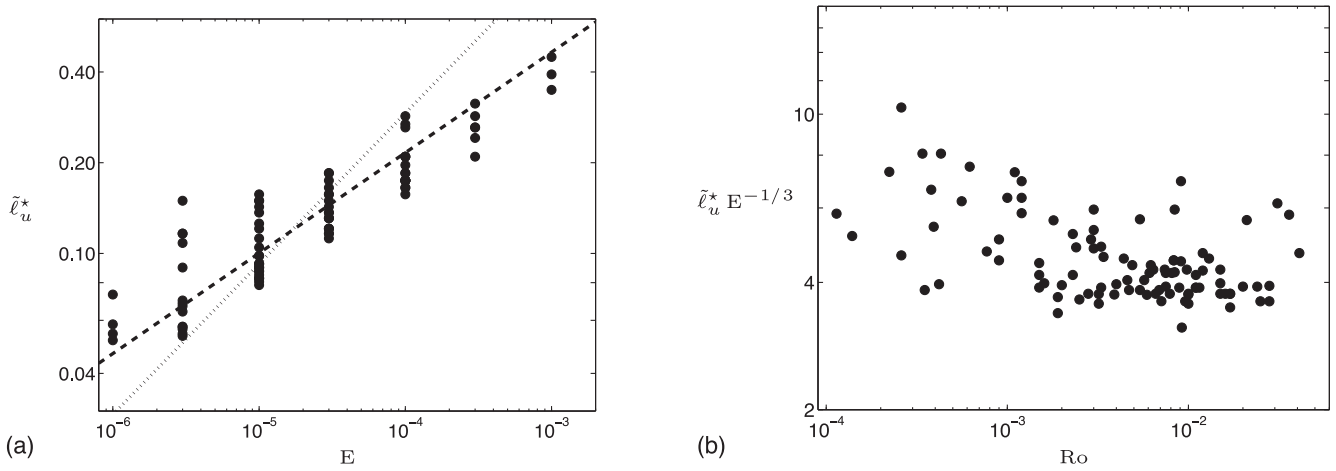

Figure 7. (a) The non-dimensional characteristic length scale $\tilde{\ell}_u^\star$ as a function of the Ekman number. The dashed line corresponds to $\tilde{\ell}_u^\star \sim \mathrm{E}^{1/3}$ (eq. 27) and the dotted line to $\tilde{\ell}_u^\star \sim \mathrm{E}^{1/2}$. (b) The corrected length scale $\tilde{\ell}_u^\star\,\mathrm{E}^{-1/3}$ as a function of the Rossby number. Similar graphs can be produced using $\ell_u^\star$ instead of $\tilde{\ell}_u^\star$. This figure relies on the full 102 dynamos database.

Coriolis force. It provides (see Petrelis & Fauve 2001) in non-dimensional form

$$\Lambda \sim (\mathrm{Rm} - \mathrm{Rm}_d)\,. \tag{29}$$

Each of the relations (26), (28) and (29) can be tested against the 42 dynamos database (see Fig. 8), and yields the relative misfits $\chi_{\mathrm{rel}} = 1.438$, $\chi_{\mathrm{rel}} = 0.891$, and $\chi_{\mathrm{rel}} = 2.081$, respectively. The best scaling law fitting the numerical data is therefore (28). It is consistent with the fact that viscous effects have been shown to play a non-negligible role in the bulk of the flow in numerical models.

This result can be compared to the output of a direct numerical fit. The values of the magnetic Reynolds number at the onset of dynamo action corresponding to seven sets of E, Pr and Pm in the database have been estimated by a linear interpolation of Lo^2 as a function of Rm (see Table 1 and Appendix E). The multiple linear regression approach applied to the 42 dynamos database provides the following scaling law for the Elsasser number Λ as a function of $(\mathrm{Rm} - \mathrm{Rm}_d)$ and E (95 per cent confidence intervals given in Table 3): [1]

$$\Lambda \simeq 10.24\,(\mathrm{Rm} - \mathrm{Rm}_d)^{1.09}\,\mathrm{E}^{0.52}, \qquad \text{with} \quad \chi_{\mathrm{rel}} = 0.698\,. \tag{30}$$

The physically derived scaling law (28) is consistent with the empirical scaling law (30) for the dependence on $(\mathrm{Rm} - \mathrm{Rm}_d)$. The optimal exponent of E is larger than the 1/3 value predicted by (28), and remains to be investigated.

Fig. 10(a) represents relation (28) applied to the 42 dynamos database in red diamonds, and the same relation, but setting Rm_d to zero in blue squares. The blue points gradually move away from a linear fit when Rm decreases, as expected (because the approximation $\mathrm{Rm} - \mathrm{Rm}_d \simeq \mathrm{Rm}$ worsens). Relation (28) can however then be applied to the 102 dynamos database, provided that the parameter Rm_d is dropped (since it is only known for the 42 simulations of the reduced database). It is represented in Fig. 10(b). As in Fig. 10(a), the full numerical database appears to follow the proposed scaling law, except for low values of Rm for which Rm_d cannot be neglected.

It is worth noting that relation (28) reveals a dependence of the magnetic field strength on viscosity, which is geophysically not realistic. To illustrate this, let us now try to apply this relation to the Earth's core. We choose the common estimate value $\mathrm{Rm} = 10^3$. The distance to the onset of dynamo action $\mathrm{Rm} - \mathrm{Rm}_d$ can be estimated by Rm, which leads to an overestimated value of Λ. We find $\Lambda \sim 10^{-2}$, which is an upper bound because Rm_d was not taken into account. It is yet much smaller than its estimated value for the Earth's core, expected to be close to unity (Roberts 1988). This indicates very clearly that available numerical models are not in the dynamical regime relevant to geodynamo. In other words, the Earth's core would simply be out of the range of Fig. 10(a) (with $\mathrm{Rm} \simeq 10^3$, and $\Lambda\,\mathrm{E}^{1/3} \simeq 10^5$).

The magnetic Reynolds number is however a measured quantity in the numerical database. In order to establish a predictive scaling for the magnetic field strength, it is thus necessary to express the flow amplitude as a function of control parameters. This is the purpose of the two next sections.

4.4 Predictive scaling law for the injected power

The definition of the output parameter $\mathrm{Ra}_Q^\star$ involves the efficiency with which heat is transferred by convection, measured by the Nusselt number Nu (see eq. 13). This is a subject of study in itself, many studies of heat transfer have been performed for rotating convection. Fig. 11 shows that the numerical data globally correspond to an intermediate regime between the rapidly rotating regime ($\mathrm{Nu} = \widetilde{R}^{6/5}$, Aurnou 2007; King *et al.* 2009, 2010) and the weakly rotating regime ($\mathrm{Nu} \sim \mathrm{Ra}^{2/7}$, see King *et al.* 2009). The simple relation $\mathrm{Nu} \sim \widetilde{R}$ provides a good description of the database. Note that in Fig. 11, a dependence on Pr remains. This could be further investigated by seeking for a dependence on $\mathrm{Pr}/(1 + \mathrm{Pr})$ (instead of a power law dependence which would lack regularity in the limit $\mathrm{Pr} \longrightarrow 0$ or $\mathrm{Pr} \longrightarrow +\infty$). As we will however discuss later (see Section 4.6), the $\mathrm{Pr}/(1 + \mathrm{Pr})$ term can be omitted without significant loss of quality in describing the present database.

[1] A direct numerical fit of Λ as a function of $(\mathrm{Rm} - \mathrm{Rm}_d)$, E, Pm and Pr yields $\Lambda \simeq 0.30\,(\mathrm{Rm} - \mathrm{Rm}_d)^{0.88}\,\mathrm{E}^{0.12}\,\mathrm{Pm}^{0.79}\,\mathrm{Pr}^{-0.82}$, with $\chi_{\mathrm{rel}} = 0.301$ (see Table 3 and Fig. 9a). The proposed dependence on Pr is not strongly constrained, since the estimation of the optimal exponent of Pr is only based on three simulations corresponding to $\mathrm{Pr} \neq 1$ (and for all three, $\mathrm{E} = 1 \times 10^{-4}$, $\mathrm{Pr} = 10$, $\mathrm{Pm} = 10$, see Table 1). The proposed dependence is therefore clearly not robust. The bias between E and Pm in the database probably accounts for the smaller exponent of E and the extra dependence on Pm in the above relation compared to (30).

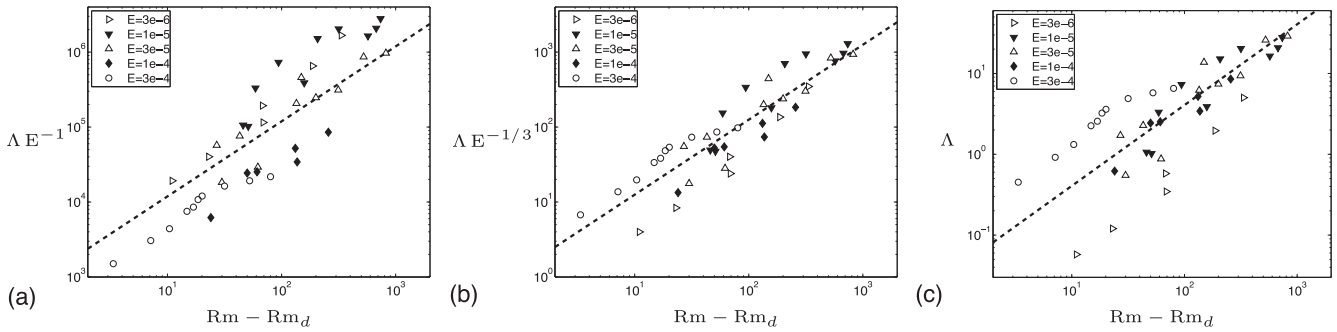

Figure 8. Scaling laws for the magnetic field strength as a function of the flow amplitude as measured by $\mathrm{Rm} - \mathrm{Rm}_d$: (a) relation (26), (b) relation (28) and (c) relation (29). This figure relies on the 42 dynamos database.

Table 2. Optimal scaling laws obtained by the multiple linear regression method, for Ra_c, $\mathrm{Ra}_Q^\star$ (relation (32) and relation given in the footnote 2), Ro (relation (36) and relation given in the footnote 3) and Rm (relation given in the footnote 4 and relation (38)) (95 per cent confidence intervals). Crosses indicate that the corresponding parameter is chosen not to enter the fit. The dashes indicate that the contribution of the corresponding parameter has been found negligible.

	Pre-factor	$\mathrm{Ra}_Q^\star$	$\widetilde{R}-1$	E	Pm	Pr	Pr/(1 + Pr)	χ_{rel}
Ra_c	17.779 ± 1.468	×	×	-1.193 ± 0.008	×	×	0.579 ± 0.030	0.061
$\mathrm{Ra}_Q^\star$	1.470 ± 0.517	×	1.774 ± 0.064	1.675 ± 0.032	–	-1.557 ± 0.061	×	0.326
$\mathrm{Ra}_Q^\star$	5.103 ± 1.550	×	1.775 ± 0.041	1.703 ± 0.021	–	-2.124 ± 0.102	1.256 ± 0.208	0.173
Ro	0.589 ± 0.133	0.466 ± 0.018	×	-0.095 ± 0.033	×	×	×	0.184
Ro	1.103 ± 0.094	0.433 ± 0.006	×	–	-0.137 ± 0.015	–	×	0.100
Rm	1.535 ± 0.371	×	0.749 ± 0.036	-0.264 ± 0.020	0.843 ± 0.030	-0.656 ± 0.035	×	0.147
Rm	2.421 ± 0.547	×	0.757 ± 0.029	-0.257 ± 0.016	0.857 ± 0.024	-0.901 ± 0.070	0.528 ± 0.139	0.108

In the available database, the bias $\mathrm{Ra} \sim \mathrm{Ra} - \mathrm{Ra}_c$ (see Section 4.1) allows us to approximate Ra by $\left(\widetilde{R}-1\right)\mathrm{Ra}_c$ in the definition (13) of $\mathrm{Ra}_Q^\star$. Injecting (24) and the above simple expression for Nu (which is admittedly not based on solid physical considerations) yields

$$\mathrm{Ra}_Q^\star \sim (\widetilde{R}-1)^2\,\mathrm{E}^{5/3}\,\mathrm{Pr}^{-2}\left(\frac{\mathrm{Pr}}{1+\mathrm{Pr}}\right)^{4/3}. \tag{31}$$

The corresponding relative misfit when applied to the 102 dynamos database is $\chi_{\mathrm{rel}} = 0.311$ and it is represented in Fig. 12(a). Note that the dependence on Pr^{-2} in (31) comes from the definition (13) of $\mathrm{Ra}_Q^\star$, whereas that on $(\mathrm{Pr}/(1+\mathrm{Pr}))^{4/3}$ results from the expression of Ra_c (relation 24).

Relation (31) can be compared to an optimized empirical fit, which provides

$$\mathrm{Ra}_Q^\star \simeq 5.10\,(\widetilde{R}-1)^{1.78}\,\mathrm{E}^{1.70}\,\mathrm{Pr}^{-2.12}\left(\frac{\mathrm{Pr}}{1+\mathrm{Pr}}\right)^{1.26},$$

$$\text{with}\quad \chi_{\mathrm{rel}} = 0.173, \tag{32}$$

(95 per cent confidence intervals are given in Table 2). Relation (31) is therefore close to providing the best fit through the numerical database.[2]

The parameter $\mathrm{Ra}_Q^\star$ varies over six orders of magnitude, while none of the control parameters varies over such a wide range (see Appendix C2). Fig. 12(b) highlights the strong dependence of $\mathrm{Ra}_Q^\star$ on the Ekman number explicited in (31). This explains the above range of variation. The control parameter $\widetilde{R}-1$ covers a much more physically realistic range.

[2] If the dependence on Pr/(1 + Pr) is omitted, it yields a larger misfit ($\chi_{\mathrm{rel}} = 0.326$), and $\mathrm{Ra}_Q^\star \simeq 1.47\,(\widetilde{R}-1)^{1.77}\,\mathrm{E}^{1.68}\,\mathrm{Pr}^{-1.56}$. Both relations would not be modified if a dependence on Pm was sought (see Table 2).

4.5 Predictive scaling laws for the flow amplitude

Several scaling laws based on different forces balances have been proposed in the literature concerning the flow amplitude (detailed in King & Buffett 2013). For simulations near the onset of dynamo action, the Lorentz force can be expected to be small. Then, balancing the curl of the buoyancy term with that of the Coriolis force yields

$$u^\star \sim \tilde{\ell}_u^{\star\,-1}\,\frac{\mathrm{P}^\star}{u^\star}, \tag{33}$$

which can be rewritten, using relation (12), as

$$\mathrm{Ro} \sim \tilde{\ell}_u^{\star\,-1/2}\,\mathrm{Ra}_Q^{\star\,1/2}. \tag{34}$$

Combining (34) and (27) leads to the Viscous–Archimedean–Coriolis (VAC) scaling proposed by King & Buffett (2013)

$$\mathrm{Ro} \sim \mathrm{Ra}_Q^{\star\,1/2}\,\mathrm{E}^{-1/6}. \tag{35}$$

Its application to the 102 dynamos database is represented in Fig. 13(a), with a relative misfit $\chi_{\mathrm{rel}} = 0.201$. It can be compared to the inertial Ro-scalings $\mathrm{Ro} \sim \mathrm{Ra}_Q^{\star\,2/5}$ (derived from the IAC balance, see Aubert *et al.* 2001; Jones 2011) and $\mathrm{Ro} \sim \mathrm{Ra}_Q^{\star\,1/3}$ (resulting from mixing length theory, see Christensen 2010) (see Fig. 13b). These three scaling laws provide descriptions of the database of comparable quality. The scaling law (27) for the length scale $\tilde{\ell}_u^\star$ however indicates that the VAC scaling (35) is more relevant to the present study than inertial scaling laws.

The direct multiple linear approach provides the following optimal scaling law expressing Ro as a function of $\mathrm{Ra}_Q^\star$ and E

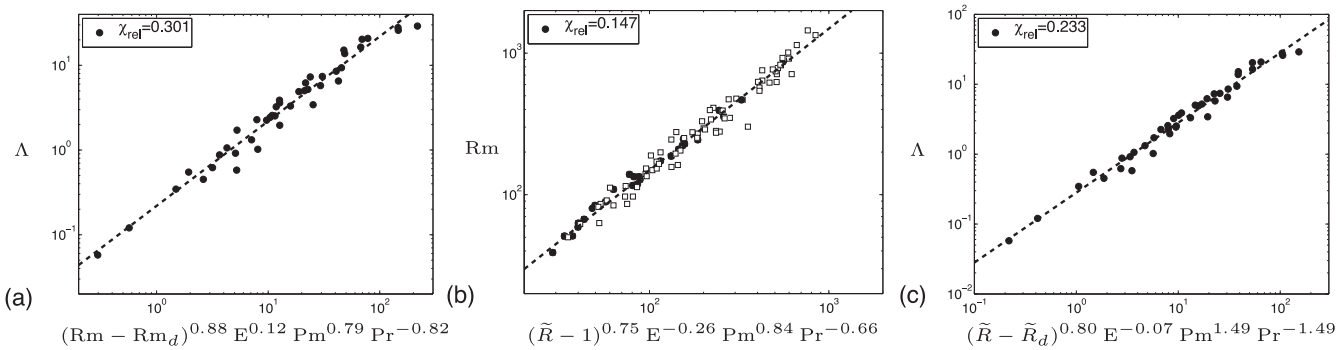

Figure 9. Scaling laws provided by direct numerical fits. (a) The Elsasser number versus the flow amplitude (see footnote 1). (b) The magnetic Reynolds number versus the normalized distance to the onset of convection (see footnote 4). (c) Predictive scaling law for the Elsasser number versus the normalized distance to the onset of dynamo action (relation 40). Squares correspond to the 102 dynamos database, black points to the 42 runs of the reduced database.

Table 3. Optimal scaling laws obtained by the multiple linear regression method, for Λ as a function of $(\mathrm{Rm}-\mathrm{Rm}_d)$ (relation (30) and relation given in footnote 1) and $(\widetilde{R}-\widetilde{R}_d)$ (relation 40) (95 per cent confidence intervals).

	Pre-factor	$\mathrm{Rm}-\mathrm{Rm}_d$	$\widetilde{R}-\widetilde{R}_d$	E	Pm	Pr	χ_{rel}
Λ	10.243 ± 8.619	1.091 ± 0.157	×	0.516 ± 0.132	×	×	0.698
Λ	0.305 ± 0.212	0.879 ± 0.087	×	0.119 ± 0.101	0.787 ± 0.141	-0.820 ± 0.174	0.301
Λ	0.351 ± 0.210	×	0.796 ± 0.062	-0.072 ± 0.071	1.490 ± 0.096	-1.491 ± 0.144	0.233

(95 per cent confidence intervals given in Table 2) [3] :

$$\mathrm{Ro} \simeq 0.59\,\mathrm{Ra}_Q^{\star\,0.47}\,\mathrm{E}^{-0.10}, \qquad \text{with} \quad \chi_{\mathrm{rel}} = 0.184\,. \tag{36}$$

Replacing the parameter $\mathrm{Ra}_Q^\star$ by its expression (31) in eq. (35) yields

$$\mathrm{Rm} \sim (\widetilde{R}-1)\,\mathrm{E}^{-1/3}\,\mathrm{Pm}\,\mathrm{Pr}^{-1}\left(\frac{\mathrm{Pr}}{1+\mathrm{Pr}}\right)^{2/3}. \tag{37}$$

This relation is essential in order to establish a predictive scaling law for the magnetic field strength, whereas relations (31) and (35) are only intermediate steps in the reasoning. Besides, the dependence of Rm on $\mathrm{E}^{-1/3}$ counterbalances the dependence of Λ on $\mathrm{E}^{1/3}$ in (28), and thus removes the dependence of Λ on viscosity in its predictive form. The scaling law (37) applied to the 102 dynamos database is represented in Fig. 14, with a relative misfit $\chi_{\mathrm{rel}} = 0.253$. The role of both terms Pr^{-1} and $[\mathrm{Pr}/(1+\mathrm{Pr})]^{2/3}$ is illustrated in Fig. 15: the term $\mathrm{Pr}/(1+\mathrm{Pr})^{2/3}$ allows to correct the data corresponding to weak values of Pr. The non-negligible dependence on $\mathrm{Pr}/(1+\mathrm{Pr})$ is consistent with previous studies of convection which established a dependence of the velocity amplitude on Pr more complex than a simple power law dependence (e.g. Schlüter *et al.* 1965; Tilgner 1996).

Finally, note that relation (37) can be compared to the optimized fit to the available data. A direct numerical fit provides [4]

$$\mathrm{Rm} \simeq 2.42\,\left(\widetilde{R}-1\right)^{0.76}\mathrm{E}^{-0.26}\mathrm{Pm}^{0.86}\mathrm{Pr}^{-0.90}\left(\frac{\mathrm{Pr}}{1+\mathrm{Pr}}\right)^{0.53},$$

$$\text{with} \quad \chi_{\mathrm{rel}} = 0.108, \tag{38}$$

[3] A direct numerical fit for Ro as a function of $\mathrm{Ra}_Q^\star$, E, Pm and Pr yields $\mathrm{Ro} \simeq 1.10\,\mathrm{Ra}_Q^{\star\,0.43}\,\mathrm{Pm}^{-0.14}$, with $\chi_{\mathrm{rel}} = 0.100$ (95 per cent confidence intervals given in Table 2). The role of E and Pr are found to be negligible. However the bias in the database (see Section 4.2) renders the dependence on Pm unreliable (as E and Pm are correlated in the database).

[4] Omitting the dependence on $\mathrm{Pr}/(1+\mathrm{Pr})$ provides a larger misfit ($\chi_{\mathrm{rel}} = 0.147$) and $\mathrm{Rm} \simeq 1.54\,\left(\widetilde{R}-1\right)^{0.75}\mathrm{E}^{-0.26}\mathrm{Pm}^{0.84}\mathrm{Pr}^{-0.66}$ (see Fig. 9b and Table 2).

(the 95 per cent confidence intervals are provided in Table 2). The exponents in relations (37) and (38) match to within 20 per cent.

4.6 Predictive scaling law for the magnetic field strength

Replacing the flow amplitude in relation (28) by its expression (37) yields the following predictive scaling law

$$\Lambda \sim (\widetilde{R}-\widetilde{R}_d)\,\mathrm{Pm}\,\mathrm{Pr}^{-1}\left(\frac{\mathrm{Pr}}{1+\mathrm{Pr}}\right)^{2/3}. \tag{39}$$

The direct numerical fit provides in the form of pure power laws

$$\Lambda \simeq 0.35\,(\widetilde{R}-\widetilde{R}_d)^{0.80}\,\mathrm{E}^{-0.07}\,\mathrm{Pm}^{1.49}\,\mathrm{Pr}^{-1.49},$$

$$\text{with} \quad \chi_{\mathrm{rel}} = 0.233, \tag{40}$$

(see Fig. 9c and Table 3 for 95 per cent confidence intervals). The dependence on the Ekman number is here negligible. Besides, we used here the reduced 42 dynamos database for which $\widetilde{R}_d$ can be estimated, the coefficients based on a direct numerical fit are therefore weakly constrained. In particular Pr does not vary much in this subsample. Despite of this, the agreement between both expressions is remarkably good, except for a larger exponent of Pm for the latter, which remains to be investigated.

The application of relation (39) to the 42 dynamos database is represented in Fig. 16(a) in red diamonds. The same expression approximating $\widetilde{R}_d$ to unity is plotted using blue squares. As expected, the quality of the approximation decreases with $\widetilde{R}$. Finally, Fig. 16(b) corresponds to the application of relation (39) to the full database, approximating the unknown $\widetilde{R}_d$ contribution to unity.

Finally, in order to assess the role of the two terms Pr^{-1} and $[\mathrm{Pr}/(1+\mathrm{Pr})]^{2/3}$ in relation (39), we compare in Fig. 17 the improvements obtained by each contribution of Pr. It highlights the important role of the Pr^{-1} term. The role of the $\mathrm{Pr}/(1+\mathrm{Pr})$ term in the description of the available numerical database is marginal (compare Figs 16b and 17b).

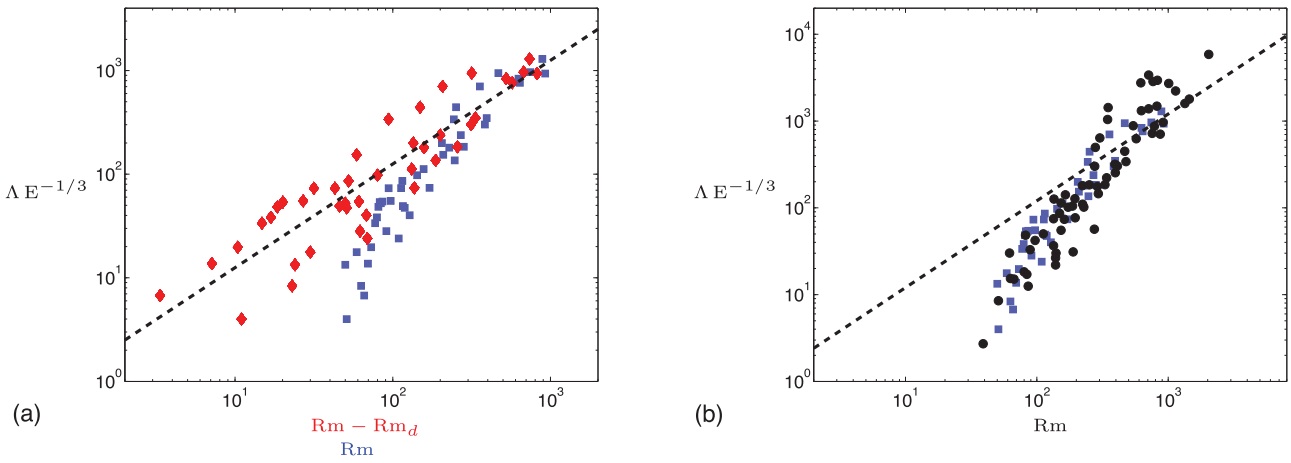

Figure 10. Physically derived relation for the magnetic field strength as a function of $\mathrm{Rm}-\mathrm{Rm}_d$. (a) Relation (28) (red diamonds), and the same relation but setting Rm_d to zero (blue squares), both applied to the 42 dynamos database. (b) Relation (28) dropping the unknown Rm_d contribution, applied to the full (blacks points) and reduced (blue squares) database. The dashed line corresponds to relation (28).

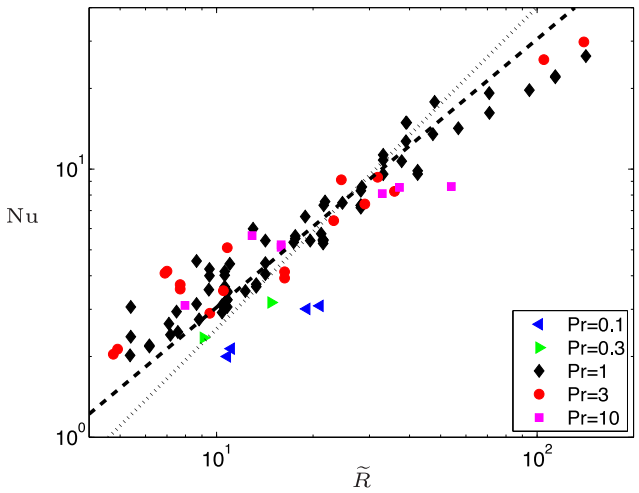

Figure 11. The Nusselt number versus the Rayleigh number normalized by its critical value. The dotted line corresponds to $\mathrm{Nu}\sim\widetilde{R}^{\,6/5}$ and the dashed line to $\mathrm{Nu}\sim\widetilde{R}$. The Prandtl number is indicated by the colour (as in Fig. 5a). This figure is based on the 102 dynamos database.

Thus, instead of the power based scaling law proposed by Christensen (2010), which can be rewritten as

$$\Lambda\sim f_{\mathrm{ohm}}\,\mathrm{Ra}_Q^{\star\,2/3}\,\mathrm{E}^{-1}\,\mathrm{Pm},\qquad\text{with}\quad\chi_{\mathrm{rel}}=0.452,\tag{41}$$

and which involves measured quantities (f_{ohm} and $\mathrm{Ra}_Q^\star$), we propose the simple relation (39), which can be reformulated as

$$\Lambda\sim(\widetilde{R}-\widetilde{R}_d)\,\mathrm{q}\left(\frac{\mathrm{Pr}}{1+\mathrm{Pr}}\right)^{2/3},\qquad\text{with}\quad\chi_{\mathrm{rel}}=0.516\,.\tag{42}$$

The $\mathrm{Pr}/(1+\mathrm{Pr})$ dependence comes from the asymptotic expression of the critical Rayleigh number at the onset of convection (24). The moderate variation of Pr in the database implies that it can be omitted without significant loss in the quality of the fit (see Fig. 17b). This provides an even simpler scaling law, valid for the available range of Pr

$$\Lambda\sim(\widetilde{R}-\widetilde{R}_d)\,\mathrm{q},\qquad\text{with}\quad\chi_{\mathrm{rel}}=0.512\,.\tag{43}$$

It involves input parameters only, and its derivation was guided by physical arguments. Besides, it is worth noting that (43) as well as (42) imply a dependence of the magnetic field amplitude on the rotation rate Ω. This contradicts earlier claims of saturation values independent on the rotation rate.

Relations (41) and (43) are applied to a reduced 33 dynamos database (for which all quantities involved in both relations are available) and represented in Fig. 18. The relative misfits given in (41), (42) and (43) are computed on the basis of this reduced database.

Note that the power based relation (41) does not involve any distance to the onset of dynamo action. Indeed, the parameter $\mathrm{Ra}_Q^\star$ does not vanish at the onset of dynamo action [it vanishes at the onset of convection, see eq. (13)]. The parameter f_{ohm} however corrects this issue, as it tends to zero at the onset of dynamo action.

5 CONCLUSION

In this study, we combine a numerical approach, which consists in establishing scaling laws for quantities of interest thanks to a multiple linear regression method applied to numerical data under the approximation of power laws, and a physical approach based either on energetics or on forces balances. Our numerical approach is based on a 102 dynamos database (U. Christensen) corresponding to Boussinesq fully convecting ($\mathrm{Nu}>2$) and dipolar dynamo models.

In a first phase, we focus our attention on scaling laws for the magnetic field strength as a function of the injected power by buoyancy forces, quantified by the flux-based Rayleigh number $\mathrm{Ra}_Q^\star$. We show that the scaling laws previously obtained in the literature mainly correspond to the simple writing of the energy balance between production and dissipation, which is necessarily valid for any dynamo in statistical equilibrium. Such power based scaling laws are thus very general and applicable to any dynamo in statistical equilibrium irrelevantly of the dynamo mechanism (e.g. Schrinner *et al.* 2012).

The description of the magnetic dissipation length scale ℓ_B determines the quality of the approximation. Assuming a constant value for ℓ_B already provides a very good description of the numerical database. Improved fits can be obtained based on finer assumptions for ℓ_B. However, none of the proposed scaling laws corresponds to a realistic physically based relation to describe the numerical database (see Section 3.4).

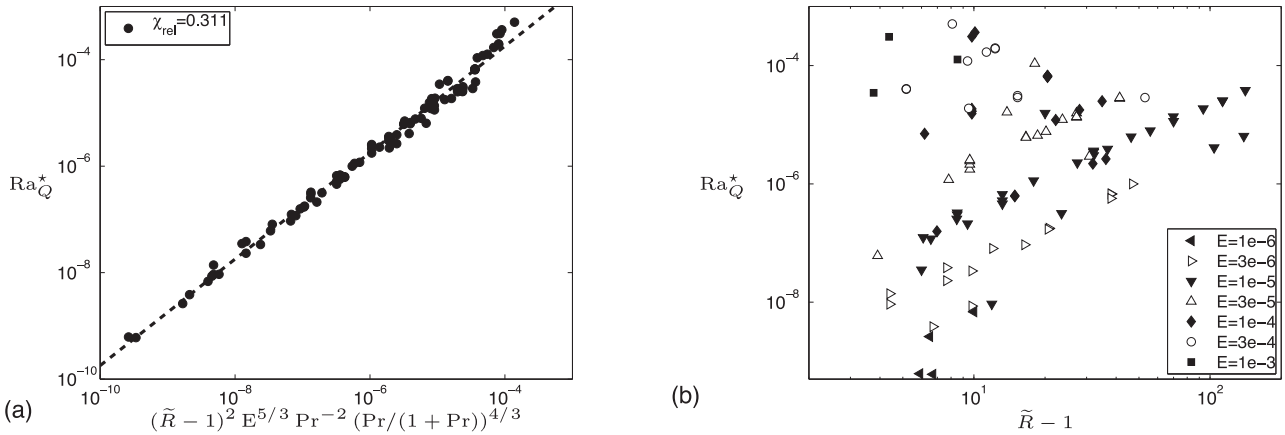

Figure 12. (a) Validation of relation (31) expressing the flux-based Rayleigh number as a function of the normalized distance to the onset of dynamo. (b) The flux-based Rayleigh number versus the normalized distance to the onset of convection. The Ekman number is indicated by using different symbols (as in Fig. 5d). This figure is based on the full 102 dynamos database.

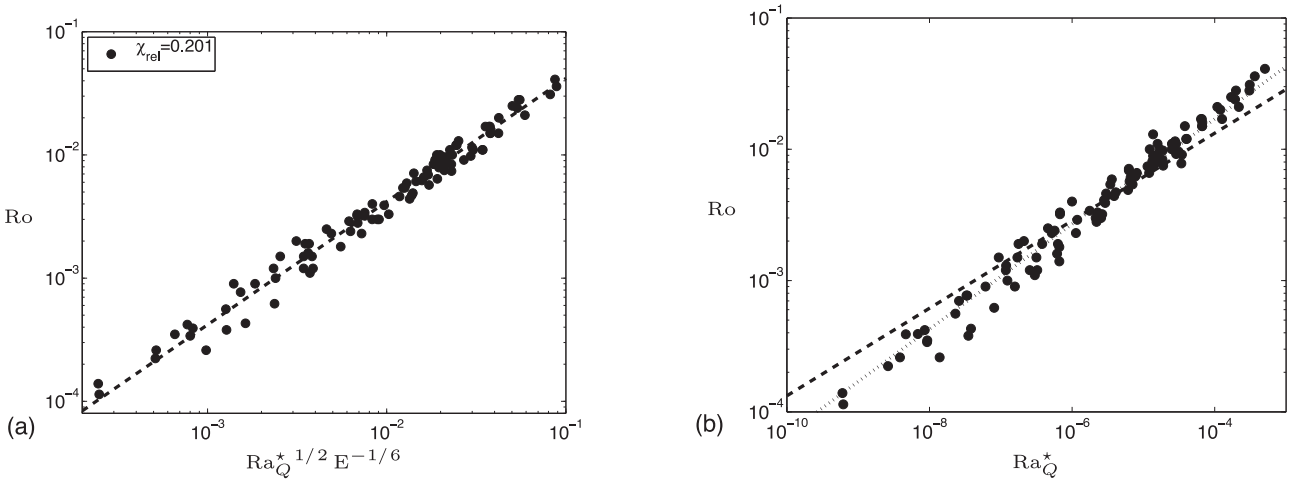

Figure 13. (a) The Rossby number as a function of the flux-based Rayleigh number (a) based on the VAC scaling (relation 35) (b) on the IAC scaling (dotted line, $\chi_{\rm rel} = 0.237$) and on the scaling resulting from mixing length theory (dashed line, $\chi_{\rm rel} = 0.431$). Both graphs rely on the full 102 dynamos database.

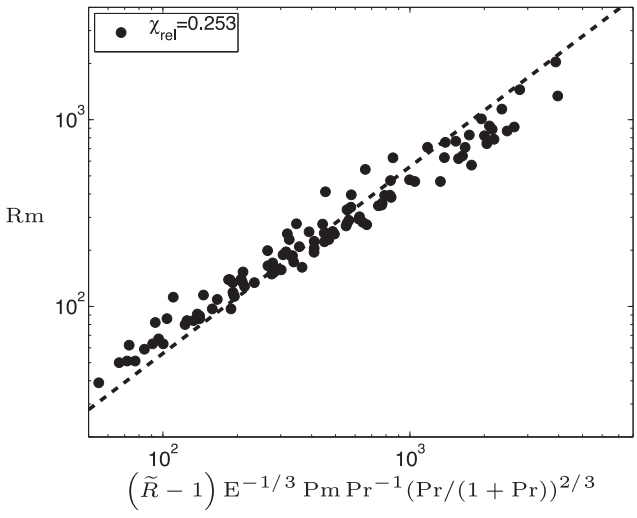

Figure 14. The resulting predictive scaling law for the magnetic Reynolds number as a function of the normalized distance to the onset of convection (relation 37). This figure relies on the full 102 dynamos database.

The second part of our study aims at establishing predictive scaling laws (i.e. as a function of input parameters only) for the magnetic field strength. Our reasoning is guided by physical arguments such as forces balances, and the numerical database is only used to validate the proposed relations. Indeed, we have shown that scaling laws obtained through a direct numerical fit can be biased by the numerical sample. It is in particular the case for the Ekman and magnetic Prandtl numbers, whose ranges are strongly correlated in the database. The flux-based Rayleigh number $\mathrm{Ra}_Q^\star$, which is a measured quantity, is replaced either by the normalized distance of the Rayleigh number to the onset of convection (denoted as $\widetilde{R} - 1$) or by the normalized distance to the onset of dynamo action (measured by $\widetilde{R} - \widetilde{R}_d$). This last quantity is unfortunately only available for a subset of the numerical database.

Our four control parameters are the Ekman number, the Prandtl number, the magnetic Prandtl number and the relative distance to the onset of convection (resp. dynamo action). Our reasoning follows four steps.

The first step of the reasoning provides a scaling law for the magnetic field strength as a function of the distance to the onset of dynamo in term of flow amplitude, which is $\Lambda \sim (\mathrm{Rm} - \mathrm{Rm}_d)\,\mathrm{E}^{1/3}$ and which matches numerical data. It is deduced from the balance

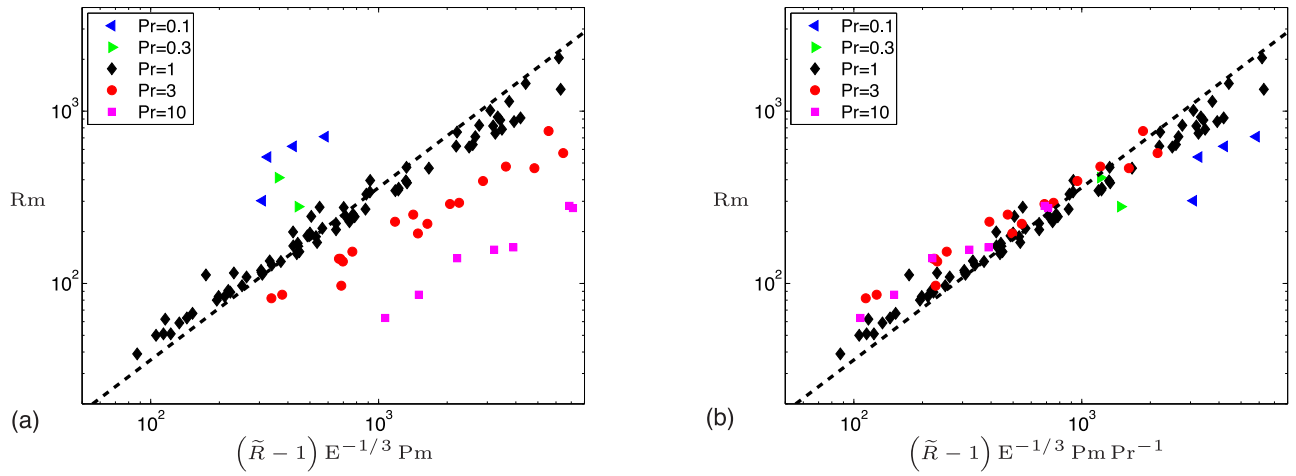

Figure 15. Simplified expressions for Rm testing the Pr dependence. The magnetic Reynolds number as a function of the normalized distance to the onset of convection, eq. (37) (a) with no correction on Pr and Pr/(1 + Pr) (b) with the correction on Pr^{-1} only. Both graphs rely on the 102 dynamos database.

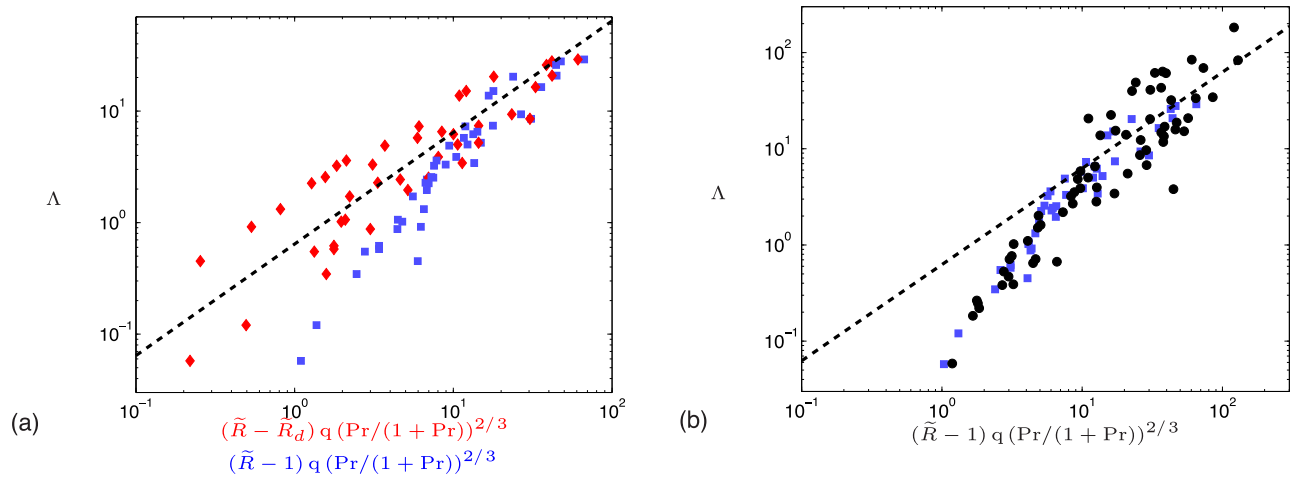

Figure 16. Physically derived predictive scaling law for the magnetic field strength as a function of $\widetilde{R}-\widetilde{R}_d$. (a) Relation (39) (red diamonds), and the same relation but approximating $\widetilde{R}_d$ to unity (blue squares), both applied to the 42 dynamos database. (b) Relation (39) approximating the unknown $\widetilde{R}_d$ contribution to unity, applied to the full (blacks points) and reduced (blue squares) database. The dashed line corresponds to relation (39).

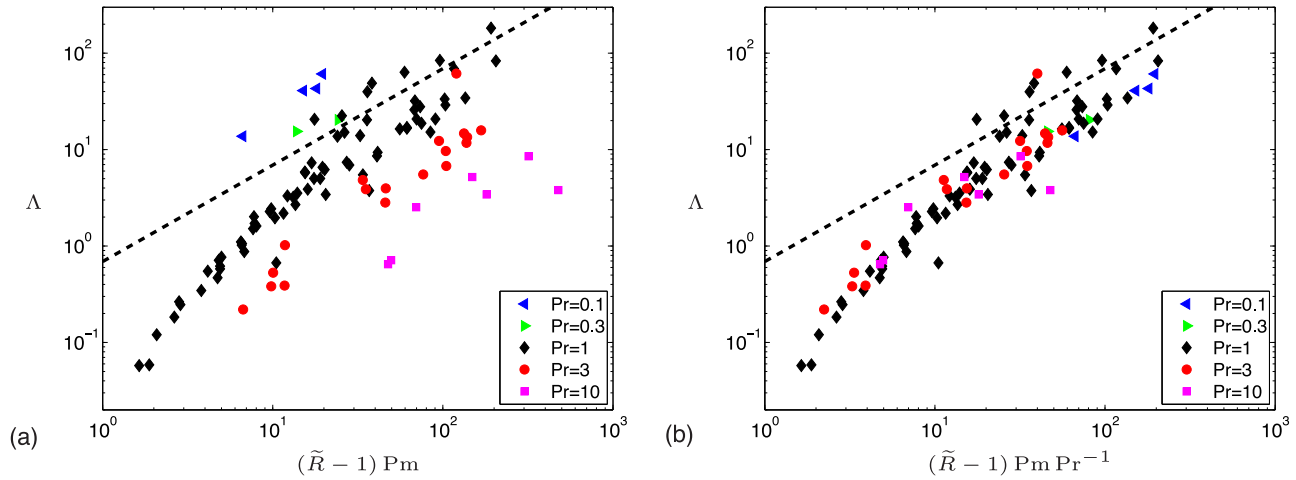

Figure 17. Test of the Pr dependence in the predictive scaling law (39) applied to the 102 dynamos database approximating the unknown $\widetilde{R}_d$ contribution to unity (a) with no correction on Pr and Pr/(1 + Pr) (b) with the correction on Pr^{-1} only. The dashed line in (a) and (b) corresponds to the scaling law (39).

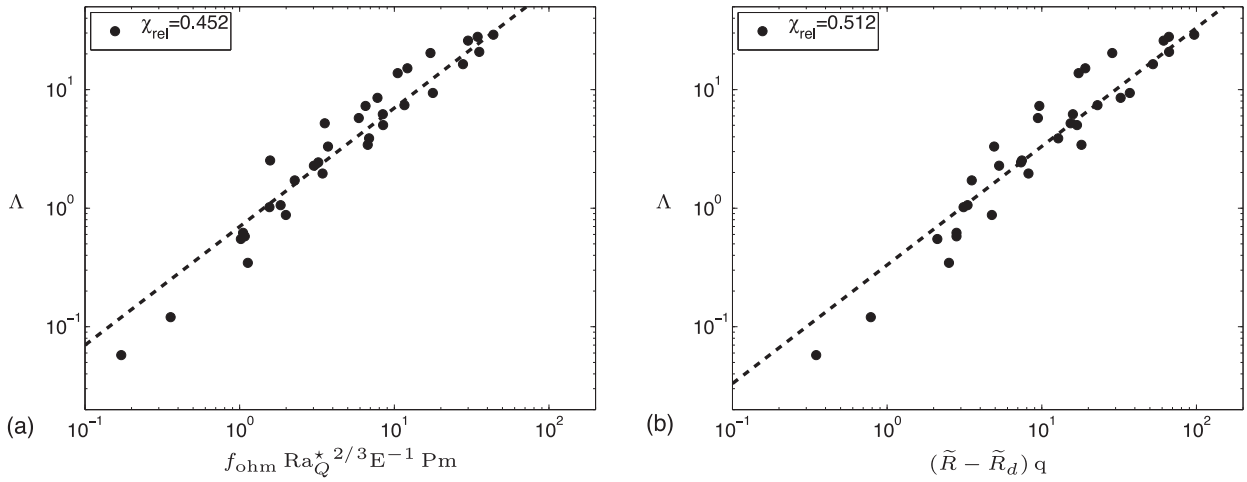

Figure 18. Comparison of the earlier power based scaling law (Christensen 2010) and our proposed predictive scaling law for the magnetic field strength: relations (a) (41) and (b) (43). Both graphs rely on a reduced 33 dynamos database for which $\widetilde{R}_d$ and $f_{\rm ohm}$ are available.

between the Lorentz force and the viscous force associated to the flow distorsion (Fauve & Petrelis 2007).

The second one consists in establishing the link between the injected power (measured by $\mathrm{Ra}_Q^\star$) and $\widetilde{R}-1$, by using the definition of $\mathrm{Ra}_Q^\star$, the relation between Nu and $\widetilde{R}$ (e.g. King *et al.* 2010) and previously established dependences of the critical Rayleigh number at the onset of convection on the Ekman and Prandtl numbers (Busse 1970).

The third step deals with the derivation of a scaling law for the flow amplitude. The Viscous–Archimedean–Coriolis scaling (King & Buffett 2013) matches the numerical data. Especially, the characteristic velocity length scale of the flow depends on $\mathrm{E}^{1/3}$ in numerical simulations, which proves that viscous effects play a non-negligible role in the bulk of the flow. The role of inertia is shown to be negligible on this length scale for dipolar dynamos compared to that of viscous effects.

Finally, in a fourth step, the combination of the aforesaid results leads to a surprisingly simple predictive scaling law, that is $\Lambda \sim (\widetilde{R}-\widetilde{R}_d)\,\mathrm{q}\,[\mathrm{Pr}/(1+\mathrm{Pr})]^{2/3}$, which involves input parameters only, contrary to previous published scaling laws, and which properly describes available numerical data (as stressed in the text, the Pr dependence is not tested by the database and can be omitted here without loss). This scaling law relies on the dominant forces balance in the numerical dynamos. Contrary to power based scaling laws, it is applicable in the parameter range covered by this study, but will not be satified in general (e.g. if inertial forces become significant). Besides its predictive power, it also provides information on the underlying forces balance at work in the dynamo simulations.

Introducing predictive scaling laws, based on control parameters only, allows to underline two important ideas. First, the present numerical models do not operate in a dominant forces balance relevant for the geodynamo. Indeed, viscous effects are shown to be essential and extrapolation to geophysically relevant parameters produces strongly underestimated amplitudes for the magnetic field. Secondly, it allows to demonstrate the clear dependence of the magnetic field strength on the rotation rate Ω.

ACKNOWLEDGEMENTS

The authors want to acknowledge stimulating discussion with Peter Davidson and gratefully thank Uli Christensen for sharing his numerical database.

REFERENCES

Aubert, J., Nataf, H.-C., Cardin, P. & Masson, J.-P., 2001. A systematic experimental study of rapidly rotating spherical convection in water and liquid gallium, *Phys. Earth planet. Int.,* **128,** 51–74.

Aurnou, J., 2007. Planetary core dynamics and convective heat transfer scaling, *Geophys. Astrophys. Fluid Dyn.,* **101**(5–6), 327–345.

Buffett, B.A., 2010. Tidal dissipation and the strength of the Earth's internal magnetic field, *Nature,* **468**(7326), 952–955.

Busse, F.H., 1970. Thermal instabilities in rapidly rotating systems, *J. Fluid Mech.,* **44**(part 3), 441–460.

Carrigan, C.R. & Busse, F.H., 1983. An experimental and theoretical investigation of the onset of convection in rotating spherical shells, *J. Fluid Mech.,* **126,** 287–305.

Chandrasekhar, S., 1961. *Hydrodynamic and Hydromagnetic stability,* Clarendon.

Christensen, U.R., 2010. Dynamo Scaling laws and applications to the planets, *Space Sci. Rev.,* **152,** 565–590.

Christensen, U.R. & Tilgner, A., 2004. Power requirement of the geodynamo from ohmic losses in numerical and laboratory dynamos, *Nature,* **429,** 169–171.

Christensen, U.R. & Aubert, J., 2006. Scaling properties of convection-driven dynamos in rotating spherical shells and application to planetary magnetic fields, *Geophys. J. Int.,* **166,** 97–114.

Christensen, U.R., Olson, P. & Glatzmaier, G.A., 1999. Numerical modelling of the geodynamo: a systematic parameter study, *Geophys. J. Int.,* **138,** 393–409.

Christensen, U.R., Holzwarth, V. & Reiners, A., 2009. Energy flux determines magnetic field strength of planets and stars, *Nature,* **457,** 167–169.

Cornillon, P.-A. & Matzner-Lober, E., 2010. *Regression Avec R,* 3rd edn, Springer.

Davidson, P.A., 2013. Scaling laws for planetary dynamos, *Geophys. J. Int.,* **195,** 67–74.

Dormy, E., Soward, A.M., Jones, C.A., Jault, D. & Cardin, P., 2004. The onset of thermal convection in rotating spheric shells, *J. Fluid Mech.,* **501,** 43–70.

Dormy, E. & Le Mouël, J.-L., 2008. Geomagnetism and the dynamo: where do we stand?, *C. R. Phys.,* **9,** 711–720.

Fauve, S. & Petrelis, F., 2007. *Mathematical Aspects of Natural Dynamos,* eds Dormy, E. & Soward, A.M., CRC Press.

Fisher, R.A., 1925. Applications of Student's distribution, *Metron,* **5,** 90–104.

Gillet, N., Jault, D., Canet, E. & Fournier, A., 2010. Fast torsional waves and strong magnetic field within the Earth's core, *Nature,* **465**(7294), 74–77.

Jones, C.A., 2011. Planetary magnetic fields and fluid dynamos, *Annu. Rev. Fluid Mech.,* **43,** 583–614.

Jones, C.A., Soward, A.M. & Mussa, A.I., 2000. The onset of thermal convection in a rapidly rotating sphere, *J. Fluid Mech.,* **405,** 157–179.
King, E.M. & Buffett, B.A., 2013. Flow speeds and length scales in geodynamo models: the role of viscosity, *Earth planet. Sci. Lett.,* **371–372,** 156–162.
King, E.M., Soderlund, K.M., Christensen, U.R., Wicht, J. & Aurnou, J.M., 2010. Convective heat transfer in planetary dynamo models, *Geochem. Geophys. Geosyst.,* **11**(6), Q06016, doi:10.1029/2010GC003053.
King, E.M., Stellmach, S., Noir, J., Hansen, U. & Aurnou, J.M., 2009. Boundary layer control of rotating convection systems, *Nature,* **457**(7227), 301–304.
Kippenham, R. & Weigert, A., 1990. *Stellar Structure and Evolution,* Springer.
Montgomery, D.C., Peck, E.A. & Vining, G.G., 2001. *Introduction to Linear Regression Analysis,* 3rd edn, John Wiley.
Morin, V. & Dormy, E., 2009. The dynamo bifurcation in rotating spherical shells, *Int. J. Mod. Phys. B,* **23**(28–29), 5467–5482.
Petrelis, F. & Fauve, S., 2001. Saturation of the magnetic field above the dynamo threshold, *Eur. Phys. J. B,* **22,** 273–276.
Roberts, P., 1968. On the thermal instability of a rotating-fluid sphere containing heat sources, *Phil. Trans. A,* **263,** 93–117.
Roberts, P., 1988. Future of geodynamo theory, *Geophys. Astrophys. Fluid Dyn.,* **44,** 3–31.
Roberts, P.H. & King, E.M., 2013. On the genesis of the Earth's magnetism, *Rep. Prog. Phys.,* **76,** 55p.
Schlüter, A., Lortz, D. & Busse, F., 1965. On the stability of steady infinite amplitude convection, *J. Fluid Mech.,* **23**(part I), 129–144.
Schrinner, M., 2013. Rotational threshold in global numerical dynamo simulations, *Mon. Not. R. astron. Soc: Lett.,* **431,** L78–L82.
Schrinner, M., Petitdemange, L. & Dormy, E., 2012. Dipole collapse and dynamo waves in global direct numerical simulations, *Astrophys. J.,* **752,** 121.
Soderlund, K.M., King, E.M. & Aurnou, J.M., 2012. The influence of magnetic fields in planetary dynamo models, *Earth planet. Sci. Lett.,* **333–334,** 9–20.
Stelzer, Z. & Jackson, A., 2013. Extracting scaling laws from numerical dynamo models, *Geophys. J. Int.,* **193,** 1265–1276.
Stevenson, D.J., 1979. Turbulent thermal convection in the presence of rotation and a magnetic field: a heuristic theory, *Astrophys. Fluid Dyn.,* **12,** 139–169.
Student, 1908. The probable error of a mean, *Biometrika,* **6,** 1–25.
Takehiro, S.-I., Ishiwatari, M., Nakajima, K. & Hayashi, Y.-Y., 2002. Linear stability of thermal convection in rotating systems with fixed heat flux boundaries, *Geophys. Astrophys. Fluid Dyn.,* **96**(6), 439–459.
Tilgner, A., 1996. High-Rayleigh-number convection in spherical shells, *Phys. Rev. E.,* **53,** 4847–4851.
Zhang, K. & Liao, X., 2004. A new asymptotic method for the analysis of convection in a rapidly rotating sphere, *J. Fluid Mech.,* **518,** 319–346.

APPENDIX A: THE MULTIPLE LINEAR REGRESSION APPROACH

As in previous studies (Christensen & Tilgner 2004; Christensen & Aubert 2006; Stelzer & Jackson 2013), we restrict our scaling analysis to power laws of the form

$$\mathbf{Y} \propto \alpha \prod_{j=1}^{p} {\mathbf{X}_j}^{\beta_j}, \tag{A1}$$

where $\mathbf{Y}$ is the n-dimensional vector of output data which we want to fit, and $\mathbf{X_j}$ are the p n-dimensional predictor variables. Taking the logarithm of (A1) transforms the model in a multiple linear regression problem

$$\mathbf{log(Y)} = \beta_0 + \beta_1 \mathbf{log(X_1)} + \beta_2 \mathbf{log(X_2)} + \cdots + \beta_p \mathbf{log(X_p)} + \boldsymbol{\varepsilon}. \tag{A2}$$

in which $\beta_0 = \log(\alpha)$, and $\boldsymbol{\varepsilon}$ in an n-dimensional vector measuring the misfit.

In the following, $\mathbf{log(Y)}$ is replaced by $\widetilde{\mathbf{Y}}$ and $\mathbf{log(X_j)}$ by $\widetilde{\mathbf{X}}_\mathbf{j}$ for clarity. The system of n equations (A2) can be represented in matrix notation as

$$\widetilde{\mathbf{Y}} = \widetilde{\mathbf{X}}\,\boldsymbol{\beta} + \boldsymbol{\varepsilon}, \tag{A3}$$

where $\widetilde{\mathbf{X}}$ is referred to as the design matrix $\left[\mathbf{I}\widetilde{\mathbf{X}}_\mathbf{1} \ldots \widetilde{\mathbf{X}}_\mathbf{p}\right]$ and $\boldsymbol{\beta}$ is a $(p+1)$-dimensional vector containing the whole set of regression coefficients. The vector $\boldsymbol{\beta}$ can be estimated using least square estimates. The misfit $\boldsymbol{\varepsilon}$ is assumed to follow a Gaussian centred distribution with a variance σ which is assumed to be a constant. The corresponding fitted model is

$$\hat{\widetilde{\mathbf{Y}}} = \widetilde{\mathbf{X}}\,\hat{\boldsymbol{\beta}}, \tag{A4}$$

where

$$\hat{\boldsymbol{\beta}} = \left(\widetilde{\mathbf{X}}^t \cdot \widetilde{\mathbf{X}}\right)^{-1} \cdot \widetilde{\mathbf{X}}^t \cdot \widetilde{\mathbf{Y}}. \tag{A5}$$

The variance σ can be estimated by the unbiased estimator $\hat{\sigma}$ defined as

$$\hat{\sigma}^2 = \frac{1}{n-p-1}\|\hat{\boldsymbol{\varepsilon}}\|^2, \qquad \text{where} \quad \hat{\boldsymbol{\varepsilon}} = \mathbf{Y} - \hat{\widetilde{\mathbf{Y}}}. \tag{A6}$$

As a measure of misfit between data and fitted values, we use as in Christensen & Aubert (2006) the mean relative misfit to the original data y_i $[i \in (1, n)]$, defined as

$$\chi_{\text{rel}} = \sqrt{\frac{1}{n}\sum_{\mathrm{i}=1}^{n}\left(\frac{y_i - \hat{y}_i}{y_i}\right)^2}. \tag{A7}$$

The estimator $\hat{\boldsymbol{\beta}}$ is unbiased and its covariance matrix can be estimated by

$$\hat{\boldsymbol{\sigma}}^2_{\hat{\boldsymbol{\beta}}} = \hat{\sigma}^2 \left(\widetilde{\mathbf{X}}^t \cdot \widetilde{\mathbf{X}}\right)^{-1}, \tag{A8}$$

which is a $(p+1) \times (p+1)$ matrix. An estimation of the variance $\hat{\sigma}_{\hat{\beta}_j}$ of the $\hat{\beta}_j$ exponent $[j \in (0, p)]$ is

$$\hat{\sigma}_{\hat{\beta}_j} = \hat{\sigma}\sqrt{\left[\left(\widetilde{\mathbf{X}}^t \cdot \widetilde{\mathbf{X}}\right)^{-1}\right]_{jj}}, \tag{A9}$$

and the estimator $(\hat{\beta}_j - \beta_j)/\hat{\sigma}_{\hat{\beta}_j}$ follows a Student distribution (Student 1908; Fisher 1925) with $(n-p-1)$ degrees of freedom. For the analysis performed in this paper, $(n-p-1) \approx 100$. In that case, the coefficient β_j is comprised in the 95 per cent confidence interval

$$\beta_j = \hat{\beta}_j \pm 2\,\hat{\sigma}_{\hat{\beta}_j}. \tag{A10}$$

This method provides the following power law for y

$$y = \exp(\hat{\beta}_0 \pm 2\,\hat{\sigma}_{\hat{\beta}_0}) \prod_{j=1}^{p} {x_j}^{\hat{\beta}_j \pm 2\hat{\sigma}_{\hat{\beta}_j}}, \tag{A11}$$

which can be rewritten as

$$y = \left[\exp(\hat{\beta}_0)\cosh(2\,\hat{\sigma}_{\hat{\beta}_0}) \pm \exp(\hat{\beta}_0)\sinh(2\,\hat{\sigma}_{\hat{\beta}_0})\right] \prod_{j=1}^{p} {x_j}^{\hat{\beta}_j \pm 2\hat{\sigma}_{\hat{\beta}_j}}. \tag{A12}$$

In this paper, the confidence intervals are provided in separated tables.

In a geometric interpretation where the essential quantity is reported in ordinate and the optimal combination of fitting parameters

in abscissa, the mean relative misfit $\chi_{\rm rel}$ measures the relative ordinate distance between observations and estimations, without taking the abscissa distance into account. That is why its use is restricted to comparisons of fits for the same quantity y. Besides, the mean relative misfit $\chi_{\rm rel}$ is obviously expected to decrease with the number p of predictor variables. As the system of equations (1–3) is governed by four non-dimensional parameters (Ra, E, Pm and Pr), the maximum number $p_{\rm max}$ of independent predictor variables is equal to 4. For further discussions on fitting errors, we refer the reader to Stelzer & Jackson (2013).

APPENDIX B: ROLE OF THE FRACTION OF OHMIC DISSIPATION $f_{\rm ohm}$ IN EMPIRICAL SCALING LAWS FOR THE MAGNETIC FIELD STRENGTH

We stress here the pifalls of direct numerical fits, free from physical insight, by showing that different *a priori* hypothesis on $f_{\rm ohm}$ yield contradictory results.

B1 Power based scaling laws derived from multiple linear regressions

As noted in Section 3.1, $f_{\rm ohm}$ is not at all a trivial parameter, as it involves both controlled and measured quantities. Indeed with our notations, eq. (5) can be rewritten as

$$f_{\rm ohm} = \left(1 + \frac{\mathrm{Ro}^2}{\mathrm{Lo}^2}\frac{{\ell_B^\star}^2}{{\ell_u^\star}^2}\,\mathrm{Pm}\right)^{-1}, \tag{B1}$$

where we introduced a kinematic dissipation length scale ℓ_u ($\ell_u^\star = \ell_u/L$), defined using time averaged quantities as

$$\ell_u^2 \equiv \frac{\int_V \mathbf{u}^2\,\mathrm{d}V}{\int_V (\nabla\times\mathbf{u})^2\,\mathrm{d}V} = 2\,\nu\frac{E_{\rm kin}}{D_\nu}\,. \tag{B2}$$

The main distinction between the scaling laws (18) and (23) respectively proposed by Christensen & Aubert (2006) and Davidson (2013) relies on the different exponent of $f_{\rm ohm}$.

First considering the best empirical scaling law for the magnetic field strength in our database, ignoring the $f_{\rm ohm}$ parameter, we get

$$\mathrm{Lo} \simeq 0.16\,{\mathrm{Ra}_Q^\star}^{0.32}\,\mathrm{E}^{-0.11}\,\mathrm{Pm}^{0.30}\,\mathrm{Pr}^{-0.18}, \qquad \text{with} \quad \chi_{\rm rel} = 0.194, \tag{B3}$$

(see Fig. B1a). Note that in the above expression, the right-hand-side vanishes at the onset of convection and not at the onset of dynamo action. This expression is therefore obviously not valid close to the onset of dynamo action.

The balance between energy production and dissipation provides an exponent 1/2 for $f_{\rm ohm}$ (see Section 3.1). The best power law approximation for Lo as a function of $\mathrm{Ra}_Q^\star$ obtained by setting the exponent of $f_{\rm ohm}$ to 1/2 is then

$$\mathrm{Lo} \simeq 0.78\,{f_{\rm ohm}}^{1/2}\,{\mathrm{Ra}_Q^\star}^{0.32}, \qquad \text{with} \quad \chi_{\rm rel} = 0.256, \tag{B4}$$

whereas allowing for a dependence on Pm leads to

$$\mathrm{Lo} \simeq 0.64\,{f_{\rm ohm}}^{1/2}\,{\mathrm{Ra}_Q^\star}^{0.31}\,\mathrm{Pm}^{0.17}, \qquad \text{with} \quad \chi_{\rm rel} = 0.141\,. \tag{B5}$$

These two expressions correspond to the fits (18) and (19) of Christensen & Aubert (2006). The exponents do not exactly match because the numerical database used here is somewhat larger. However, the two latter relations are rigorously recovered if we apply our algorithm to the 65 dynamos numerical database of Christensen & Aubert (2006). This validates the multiple linear regression approach used in this paper. The role of the parameter Pr is found to be negligible using the 65 dynamos numerical database of Christensen & Aubert (2006). But the 102 dynamos database used here contains more simulations corresponding to $\mathrm{Pr} \neq 1$ than the earlier Christensen & Aubert (2006) database (32 versus 17). Considering an additional dependence on Pr yields

$$\mathrm{Lo} \simeq 0.56\,{f_{\rm ohm}}^{1/2}\,{\mathrm{Ra}_Q^\star}^{0.30}\,\mathrm{Pm}^{0.20}\,\mathrm{Pr}^{-0.11}, \qquad \text{with} \quad \chi_{\rm rel} = 0.121, \tag{B6}$$

(see Fig. B1b), where the dependence on Pr is not negligible. On the contrary, the contribution of the Ekman number appears negligible (taking E into account only provides a very minor improvement of $\chi_{\rm rel}$ and a small power of E).

It is however natural in a fitting approach to let the exponent $f_{\rm ohm}$ be determined by the multiple linear regression approach. Moreover, as noted above, the $f_{\rm ohm}$ parameter is usually argued to be equal to unity in planetary dynamos. The best power law with the above parameters is

$$\mathrm{Lo} \simeq 0.66\,{f_{\rm ohm}}^{0.61}\,{\mathrm{Ra}_Q^\star}^{0.31}\,\mathrm{Pm}^{0.19}\,\mathrm{Pr}^{-0.08}, \qquad \text{with} \quad \chi_{\rm rel} = 0.117, \tag{B7}$$

(see Fig. B1c). The contribution of E is negligible, this last relation thus involves five non-dimensional parameters only, which corresponds to the maximum number of independent parameters in the problem (see Appendix A). Table B1 gathers the fitted values corresponding to equations (B3), (B4), (B5), (B6) and (B7) including their 95 per cent confidence interval. The exponents in relation (B7)

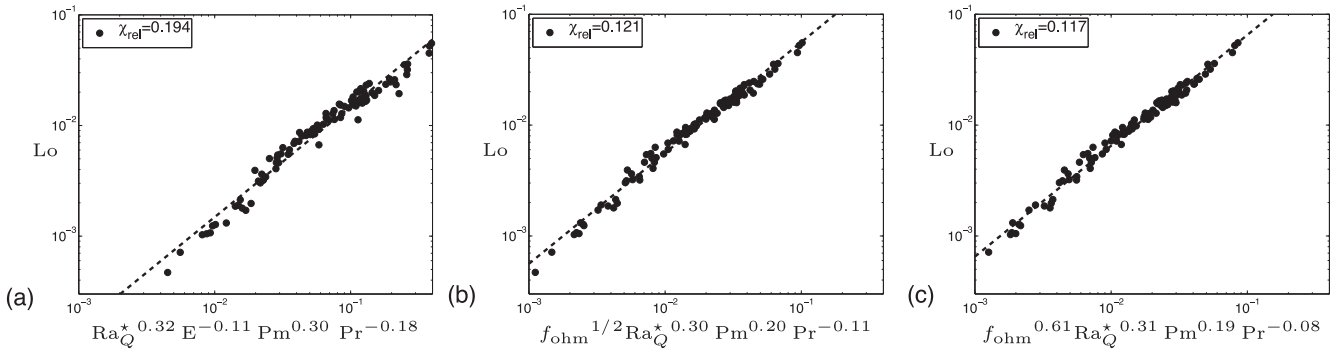

Figure B1. The Lorentz number versus a combination of flux-based Rayleigh number, Ekman number, Prandtl number, magnetic Prandtl number (a) with no $f_{\rm ohm}$ dependence (eq. B3), (b) with an additional fixed ${f_{\rm ohm}}^{1/2}$ factor (eq. B6) and (c) an additional $f_{\rm ohm}$ dependence with an optimized exponent (eq. B7). This figure relies on the 102 dynamos database.

Table B1. Optimal scaling laws obtained by the multiple linear regression method, for Lo and $f_{\rm ohm}$ (95 per cent confidence intervals): relations (B3), (B4), (B5), (B6), (B7) and (B8).

	Pre-factor	$f_{\rm ohm}$	$\mathrm{Ra}^\star_Q$	E	Pm	Pr	$\chi_{\rm rel}$
Lo	0.157 ± 0.050	$\times$	0.318 ± 0.027	-0.111 ± 0.053	0.295 ± 0.039	-0.176 ± 0.056	0.194
Lo	0.777 ± 0.168	1/2	0.322 ± 0.017	$\times$	$\times$	$\times$	0.256
Lo	0.638 ± 0.080	1/2	0.313 ± 0.009	$\times$	0.167 ± 0.023	$\times$	0.141
Lo	0.561 ± 0.063	1/2	0.302 ± 0.009	–	0.197 ± 0.021	-0.106 ± 0.033	0.121
Lo	0.661 ± 0.114	0.605 ± 0.091	0.309 ± 0.010	–	0.186 ± 0.023	-0.080 ± 0.039	0.117
$f_{\rm ohm}$	0.073 ± 0.026	$\times$	–	-0.170 ± 0.030	0.180 ± 0.042	-0.178 ± 0.054	0.249

Table B2. 95 per cent confidence intervals associated to exponents in the dimensional scaling laws for the magnetic field strength corresponding to relations (B9), (B10) and (B11).

	P	Ω	L	ρ	ν	η	κ	$\chi_{\rm rel}$
$\mathrm{B}/\mu^{1/2}$	0.318 ± 0.027	0.157 ± 0.134	-0.368 ± 0.241	0.182 ± 0.027	0.008 ± 0.142	-0.295 ± 0.039	0.176 ± 0.056	0.194
$\mathrm{B}/\mu^{1/2}$	0.302 ± 0.009	0.094 ± 0.027	-0.510 ± 0.045	0.198 ± 0.009	0.091 ± 0.054	-0.197 ± 0.021	0.106 ± 0.033	0.121
$\mathrm{B}/\mu^{1/2}$	0.309 ± 0.010	0.073 ± 0.030	-0.545 ± 0.050	0.191 ± 0.010	0.106 ± 0.062	-0.186 ± 0.023	0.080 ± 0.039	0.117

are not significantly different from those in relation (B6). In particular, the 95 per cent confidence interval associated to the optimized value 0.61 of the exponent of $f_{\rm ohm}$ in (B7) includes the value 1/2 provided by the energy balance.

The relative error on the exponents of $\mathrm{Ra}^\star_Q$, Pm and $f_{\rm ohm}$ is in general moderate (less than 15 per cent). The error for the estimation of the exponent of Pr is more important (between 30 per cent and 50 per cent): the distribution of the control parameter Pr in our data set, although wider than in the data set used in Christensen & Aubert (2006), is indeed not wide enough to establish a clear dependence on Pr. The parameter E appears only in relation (B3) where the output parameter $f_{\rm ohm}$ is not taken into account, with a relative error of 50 per cent for the corresponding exponent.

Finally, note that eqs (B3), (B6) and (B7) can be related by introducing the best power law approximation for $f_{\rm ohm}$ as a function of $\mathrm{Ra}^\star_Q$, E, Pm and Pr, that is

$$f_{\rm ohm} \simeq 0.07\,\mathrm{E}^{-0.17}\,\mathrm{Pm}^{0.18}\,\mathrm{Pr}^{-0.18}, \qquad \text{with} \quad \chi_{\rm rel} = 0.249, \tag{B8}$$

where the contribution of $\mathrm{Ra}^\star_Q$ is found to be negligible (95 per cent confidence intervals in Table B1). The high corresponding relative misfit (25 per cent) reveals that the dependence of $f_{\rm ohm}$ on other parameters can not be reliably approximated by a simple power law.

B2 Extrapolation to natural dynamos

The results of Appendix B1 deserve careful analysis. Eq. (B7) may be indeed viewed as a minor improvement in the quality of the fit, resulting from the introduction of an additional degree of freedom in the problem. Besides, the $f_{\rm ohm}$ parameter involves most of the quantities we are trying to fit, that is to say Lo, Ro, $\ell^\star_B$ and $\ell^\star_u$ (see eq. B1).

Nevertheless, the above study clearly indicates that different scaling laws can be proposed for Lo, depending on exponents considered for $f_{\rm ohm}$. If one adopts the usual assumption that $f_{\rm ohm} = 1$ for planetary applications, the resulting relation for such applications will not depend on the exponent of $f_{\rm ohm}$. To illustrate this, we can write equations (B3), (B6) and (B7) in dimensional form assuming $f_{\rm ohm} = 1$. These are, respectively,

$$\mathrm{B} \sim \mu^{1/2}\,\mathrm{P}^{0.32}\,\Omega^{0.16}\,L^{-0.37}\,\rho^{0.18}\,\nu^{0.01}\,\eta^{-0.30}\,\kappa^{0.18}, \quad \text{with} \quad \chi_{\rm rel} = 0.194, \tag{B9}$$

$$\mathrm{B} \sim \mu^{1/2}\,\mathrm{P}^{0.30}\,\Omega^{0.09}\,L^{-0.51}\,\rho^{0.20}\,\nu^{0.09}\,\eta^{-0.20}\,\kappa^{0.11}, \quad \text{with} \quad \chi_{\rm rel} = 0.121, \tag{B10}$$

and

$$\mathrm{B} \sim \mu^{1/2}\,\mathrm{P}^{0.31}\,\Omega^{0.07}\,L^{-0.55}\,\rho^{0.19}\,\nu^{0.11}\,\eta^{-0.19}\,\kappa^{0.08}, \quad \text{with} \quad \chi_{\rm rel} = 0.117\,. \tag{B11}$$

Table B2 gathers the above fitted values and the corresponding confidence intervals. The latter are calculated using the 95 per cent confidence intervals found in the non-dimensional scaling laws, considering their more pessimistic combination. By this process, the three relations can not be distinguished: for the exponents of all parameters, there exists an interval common to the three expressions. However, if we consider 70 per cent confidence intervals as Stelzer & Jackson did, the incertitude of the exponent $\hat{\beta}_j$ is equal to $\hat{\sigma}_{\hat{\beta}_j}$ instead of $2\,\hat{\sigma}_{\hat{\beta}_j}$ (see Appendix A). We can also deduce that expression (B9) predicts a dependence of B on Ω which is twice that of (B11). A similar effect can be noted for the dependence on κ. The dependence on η predicted by (B9) is also 1.5 higher than that predicted by the scaling law (B11). Finally, (B9) predicts a much weaker dependence on ν than (B11) (1/10th factor). Thus, in the limit of 70 per cent confidence intervals, the dependence of the magnetic field strength on physical parameters seems to depend on the role given to $f_{\rm ohm}$ in the numerical fit.

Using an estimate for the Earth's core of $\mathrm{Ra}^\star_{Q\,\mathrm{Earth}} = 10^{-14}$ (e.g. Christensen & Aubert 2006) in (B3), (B6) and (B7) yields $\mathrm{B}_{\mathrm{Earth}} = 0.10$ mT, $\mathrm{B}_{\mathrm{Earth}} = 0.05$ mT and $\mathrm{B}_{\mathrm{Earth}} = 0.05$ mT, respectively. It should be compared to the rms magnetic field strength inside the Earth's core, estimated to be of the order of $2 - 4$ mT (e.g. see Buffett 2010; Gillet *et al.* 2010). Our values above are lower than this estimated value by a factor 20–40, just as the values obtained by Christensen & Aubert (2006) and Stelzer & Jackson (2013).

APPENDIX C: THE MAGNETIC DISSIPATION LENGTH SCALE ℓ_B

C1 The ℓ_B length scale as a function of the flow amplitude

We interpret here earlier scaling laws in terms of assumptions made on $\ell^\star_B$ and their implications for Ro and $\ell^\star$.

Christensen & Tilgner (2004) have empirically shown that $\tau^\star_\eta \sim \mathrm{Rm}^{-1}$. Because $\tau^\star_\eta \sim {\ell^\star_B}^2$, this provides $\ell^\star_B \sim \mathrm{Rm}^{-1/2}$ (see

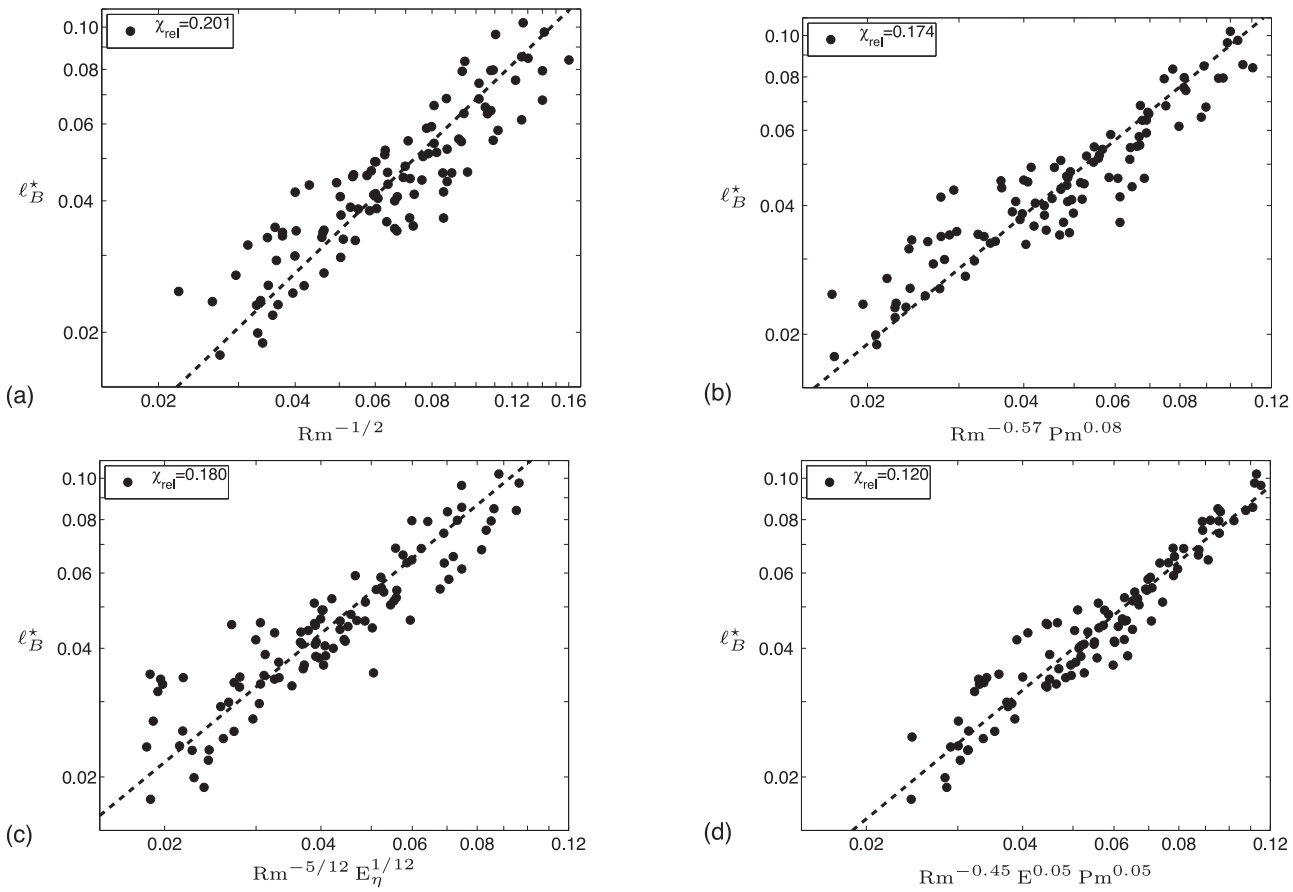

Figure C1. The magnetic dissipation length scale versus a combination of the magnetic Reynolds number, the Ekman number and the magnetic Prandtl number: (a) $\ell_B^\star \sim \mathrm{Rm}^{-1/2}$ (b) $\ell_B^\star \sim \mathrm{Rm}^{-0.57}\,\mathrm{Pm}^{0.08}$ (both derived from Christensen & Tilgner 2004) (c) $\ell_B^\star \sim \mathrm{Rm}^{-5/12}\,\mathrm{E}_\eta^{1/12}$ (Christensen 2010) (d) $\ell_B^\star \sim \mathrm{Rm}^{-0.45}\,\mathrm{E}^{0.05}\,\mathrm{Pm}^{0.05}$ (Stelzer & Jackson 2013). These graphs rely on the full 102 dynamos database.

fig. C1a, see also Roberts & King 2013). According to eq. (16), this scaling law corresponds to assuming that $\ell^\star \sim 1$, that is, ℓ is the width of the spherical shell. It is reasonably consistent with the 102 dynamos database used in this paper, since $\mathrm{Rm}\ell_B^{\star\,2}$ varies from 0.19 to 1.25, that is to say over about one order of magnitude. Moreover, note that some of the values are higher than unity: it is symptomatic of the role played by correlations between the norm and direction of **u** and **B**. Christensen & Tilgner (2004) have empirically improved the above scaling law to $\ell_B^\star \sim \mathrm{Rm}^{-0.49}\,\mathrm{Re}^{-0.08}$, where Re is the Reynolds number ($\mathrm{Re} = \mathrm{Rm}\,\mathrm{Pm}^{-1}$). This expression can be reformulated as $\ell_B^\star \sim \mathrm{Rm}^{-0.57}\,\mathrm{Pm}^{0.08}$ (see Fig. C1b). Thanks to a larger numerical data sample, this last scaling law has been optimised by Christensen (2010) as $\ell_B^\star \sim \mathrm{Rm}^{-5/12}\,\mathrm{E}_\eta^{1/12}$ (see Fig. C1c), and then by Stelzer & Jackson (2013) as $\ell_B^\star \sim \mathrm{Rm}^{-0.45}\,\mathrm{E}^{0.05}\,\mathrm{Pm}^{0.05}$ (see Fig. C1d).

As expected, the relative misfit χ_{rel} decreases when the number of predictor variables increases. Moreover, note that fits in Fig. C1 are based on 102 numerical simulations extracted from the data sample provided by U. Christensen. Thus, the sample used in Fig. C1 is larger than the one originally used by Christensen & Tilgner (2004) and Christensen (2010), and slightly different from that used by Stelzer & Jackson 2013, also based on the 185 dynamos database of U. Christensen but including $f_{\mathrm{dip}} > 0.35$ dynamos.

Finally, whereas the simple scaling law used in Fig. C1(a) corresponds to a simple physical assumption on the length scale ℓ, the three other laws, albeit more accurate, are simply based on empirical fits.

C2 The ℓ_B length scale as a function of the injected power

Whereas the four aforesaid scaling laws rely on the magnetic Reynolds number, scaling laws for the magnetic field amplitude based on a production/dissipation balance rely on the flux-based Rayleigh number $\mathrm{Ra}_Q^\star$ (see Sections 3.1 and 3.2). It is therefore natural to seek for relations between the dissipation length scale $\ell_B^\star$ and $\mathrm{Ra}_Q^\star$.

Indeed, published scaling laws for the amplitude of the magnetic field, such as the empirical scaling laws of Christensen & Aubert (2006) (see our eqs (18) and (19)), can readily be translated in terms of scaling laws for $\ell_B^\star$. Thus, using equations (10) and (12), the scaling laws (18) and (19), respectively imply $\ell_B^\star \sim {\mathrm{Ra}_Q^\star}^{-0.16}\,\mathrm{E}_\eta^{1/2}$, and $\ell_B^\star \sim {\mathrm{Ra}_Q^\star}^{-0.18}\,\mathrm{E}^{1/2}\,\mathrm{Pm}^{-0.39}$. It is interesting to note that in the representations of relations (18) and (19) by Christensen & Aubert (2006), the x-coordinate varies over six orders of magnitude (see Figs 2a and b in this paper and figs 8–9 in Christensen & Aubert 2006) while none of the control parameters varies over such a wide range. Thus, Fig. 3 (i.e. the above two relations) offers a somewhat more challenging representation of the very same expressions (18) and (19) in so far as the axes vary on a smaller range.

The above scaling laws expressing $\ell_B^\star$ as a function of $\mathrm{Ra}_Q^\star$ were deduced from (18) and (19). As $\ell_B^\star$ is related to both $\ell^\star$ and Ro, they also imply relations between these two parameters and $\mathrm{Ra}_Q^\star$. It is through these relations that the first of these scaling laws for the magnetic field strength was originally physically interpreted by

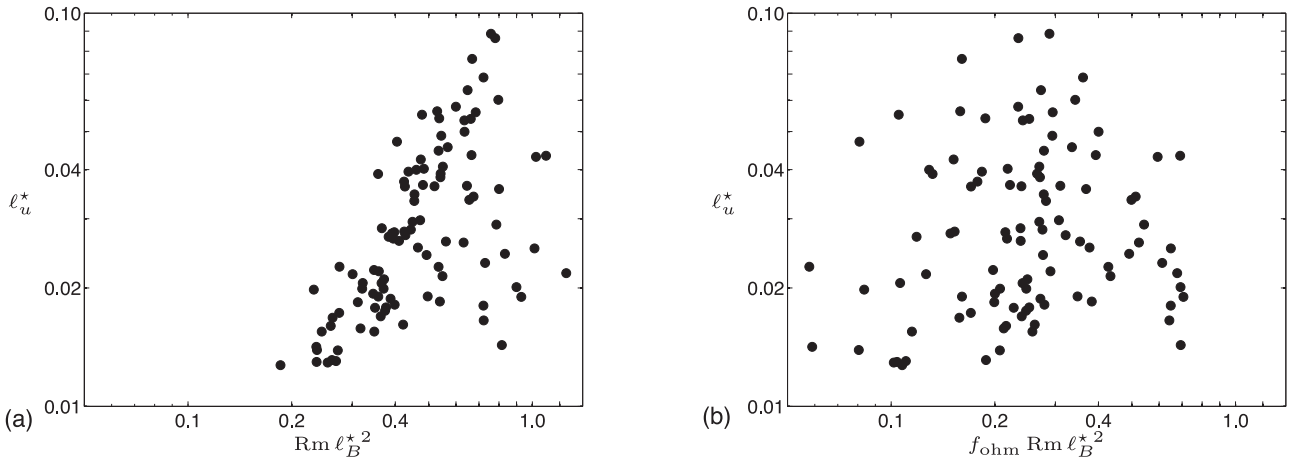

Figure D1. The length scale $\ell_u^\star$ as a function of (a) $\mathrm{Rm}\,\ell_B^{\star\,2}$ (relation D2) (b) $f_{\mathrm{ohm}}\,\mathrm{Rm}\,\ell_B^{\star\,2}$ (relation D3). These two graphs rely on the 102 dynamos database. This figure highlights that the hypothesis made by Davidson (2013), although well suited for planetary dynamos, are not met by numerical models.

Christensen & Aubert (2006), Christensen (2010) and Jones (2011) (see Section 3.4).

APPENDIX D: LENGTH SCALES IN DAVIDSON'S (2013) DEMONSTRATION

The magnetic dissipation length scale denoted as ℓ_B in the present paper is referred to as ℓ_{min} in Davidson (2013). Besides, he carefully introduced two length scales $\ell_\parallel$ and $\ell_\perp$ (the integral length scales parallel and perpendicular to the rotation axis). The length scale $\ell_\parallel$ can be approximated by L, and the length scale $\ell_\perp$ corresponds to ℓ_u introduced in the present paper in Appendix B1. Davidson (2013) is interested in planetary dynamos, for which $f_{\mathrm{ohm}} \simeq 1$. We consider here the question of the applicability of his analytical results to the length scales computed from the numerical database.

Davidson's dimensional analysis leading to relation (21) is based on the assumption that ℓ_B^2/η is independent on the rotation rate. This assumption, which was made in the limit relevant to planetary interiors, does not seem to extend to the parameter regime of numerical models. Indeed, using (9), the scaling law (B9) for the magnetic field strength implies

$$\frac{\ell_B^2}{\eta} \sim \Omega^{0.314\pm0.268}, \tag{D1}$$

(95 per cent confidence interval). Admittedly, the relative confidence interval is large, but the non-dependence of ℓ_B^2/η on the rotation rate, while sensible in the regime relevant to the geodynamo, is not relevant to the numerical data used here.

Besides, neglecting viscous effects, he considered the balance of the curl of the Coriolis force, the buoyancy force and the Lorentz force (the so-called MAC-balance, i.e. his eq. 10). Its combination with relation (21) provided by his dimensional analysis leads to $\ell_B^2 \sim \eta u^{-1} \ell_\perp$, which can be rewritten in its non-dimensional form as

$$\ell_\perp^\star \sim \mathrm{Rm}\,\ell_B^{\star\,2}. \tag{D2}$$

By comparison with eq. (16), that means that $\ell_\perp$ corresponds to our length scale ℓ defined in Section 3.3. The distinction between ℓ and $\ell_\perp$ is proved important in our study. Fig. D1(a) highlights that they should not be confused. The two assumptions, $f_{\mathrm{ohm}} \simeq 1$ and negligible viscous effects, are indeed not verified in numerical experiments.

If we use eq. (22) (eq. 9 in Davidson 2013) rather than (21) (eq. 6 in Davidson 2013) to take f_{ohm} into account, we get $\ell_B^2 \sim \eta\, f_{\mathrm{ohm}}{}^{-1}\, u^{-1}\, \ell_\perp$, which can be rewritten in its non-dimensional form as

$$\ell_\perp^\star \sim f_{\mathrm{ohm}}\,\mathrm{Rm}\,\ell_B^{\star\,2}. \tag{D3}$$

This expression corresponds to a modified form of relation (D2), adapted to $f_{\mathrm{ohm}} < 1$ cases. Fig. D1(b) shows that even such an f_{ohm} dependence does not provide a good description of the numerical data. This confirms that the assumption of negligible viscous effects, valid in the bulk of the Earth's core, is not applicable to present numerical simulations. Davidson's study therefore relies on assumptions relevant to the geodynamo, but not to present direct numerical simulations.

APPENDIX E: ESTIMATION OF THE ONSET OF DYNAMO ACTION

The critical values at the onset of dynamo action Ra_d gathered in Table 1 have been estimated through a linear interpolation of the magnetic energy as a function of the Rayleigh number near the onset of dynamo action (see Section 4.1). As underlined by Morin & Dormy (2009), the dynamo bifurcation can be either supercritical or subcritical (or take the form of isola), the nature of the bifurcation depending on the parameters. The estimation of the critical Rayleigh number in the former case is represented in Fig. E1(a): the linear interpolation of data near the dynamo threshold provides Ra_d. In the case of subcritical bifurcations, the critical Ra_d estimated by our method corresponds to the continuation of the subcritical branch, as shown in Fig. E1(b). A similar approach is used to determine Rm_d.

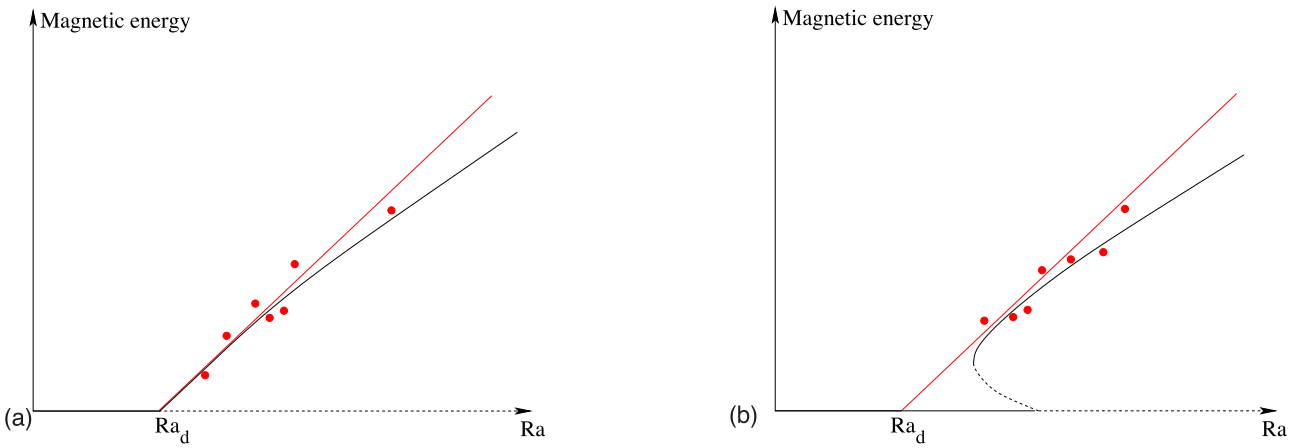

Figure E1. Schematic representation of the behaviour of the magnetic energy as a function of the Rayleigh number, for a (a) supercritical and (b) subcritical dynamo bifurcation. The solid (resp. dashed) lines indicate stable (resp. unstable) branches (see Morin & Dormy 2009). The linear interpolation (red solid line) associated to data (red points) provides the value of Ra_d in both cases.